

Cerebrospinal Fluid Flow

Douglas H. Kelley¹ and John H. Thomas²

¹Department of Mechanical Engineering, University of Rochester, Rochester, New York, USA; email: d.h.kelley@rochester.edu

²Department of Mechanical Engineering and Department of Physics and Astronomy, University of Rochester, Rochester, New York, USA; email: thomas@me.rochester.edu

 ANNUAL
REVIEWS CONNECT

www.annualreviews.org

- Download figures
- Navigate cited references
- Keyword search
- Explore related articles
- Share via email or social media

Annu. Rev. Fluid Mech. 2023. 55:237–64

First published as a Review in Advance on
September 28, 2022

The *Annual Review of Fluid Mechanics* is online at
fluid.annualreviews.org

<https://doi.org/10.1146/annurev-fluid-120720-011638>

Copyright © 2023 by the author(s). This work is licensed under a Creative Commons Attribution 4.0 International License, which permits unrestricted use, distribution, and reproduction in any medium, provided the original author and source are credited. See credit lines of images or other third-party material in this article for license information.



Keywords

biological fluid mechanics, cerebrospinal fluid, viscous flow, glymphatic system

Abstract

Circulation of cerebrospinal fluid and interstitial fluid around the central nervous system and through the brain transports not only those water-like fluids but also any solutes they carry, including nutrients, drugs, and metabolic wastes. Passing through brain tissue primarily during sleep, this circulation has implications for neurodegenerative disorders including Alzheimer's disease, for tissue damage during stroke and cardiac arrest, and for flow-related disorders such as hydrocephalus and syringomyelia. Recent experimental results reveal several features of this flow, but other aspects are not fully understood, including its driving mechanisms. We review the experimental evidence and theoretical modeling of cerebrospinal fluid flow, including the roles of advection and diffusion in transporting solutes. We discuss both local, detailed fluid-dynamic models of specific components of the system and global hydraulic models of the overall network of flow paths.

Cerebrospinal fluid (CSF): the water-like fluid in which the brain and spinal cord are immersed

Interstitial fluid (ISF): the water-like fluid filling extracellular spaces between cells in brain tissue, contiguous with and chemically indistinguishable from CSF

Extracellular space (ECS): space between cells in brain tissue, filled with ISF (not including perivascular spaces)

1. INTRODUCTION

This review focuses on the flow of cerebrospinal fluid (CSF) and interstitial fluid (ISF) in the central nervous system, including the brain and the spinal cord, as well as the combined effects of advection and diffusion associated with these flows. Taken as a whole, these fluid mechanical processes constitute a fluid and solute transport system that spans the central nervous system and operates in addition to, and in concert with, the cardiovascular system. This fluid transport system plays a role analogous to that of the lymph system that pervades the rest of the body. The components and mechanisms of CSF and ISF circulation in the brain itself are often called the glymphatic system. Its operation is important for the delivery of nutrients and for the removal of metabolic waste products, with relevance to neurodegenerative disorders including Alzheimer's disease. CSF flow in the nervous system also offers routes for delivering therapeutic drugs that do not readily cross the blood–brain barrier (BBB). Although blood flow in the brain is not the focus of this review, and we refer readers to excellent prior reviews of blood fluid mechanics (Ku 1997, Freund 2014, Secomb 2017), we show that the brain's cardiovascular system is tightly coupled to its CSF/ISF circulation system. CSF flow is necessarily shaped by the biological and anatomical properties of the central nervous system, which are introduced in this review only to the extent necessary for understanding the fluid mechanics; for more thorough discussions, we refer readers to more general reviews (Hladky & Barrand 2014, 2018, 2022; Linninger et al. 2016; Benveniste et al. 2019; Ray & Heys 2019; Mestre et al. 2020b; Kelley 2021; Bohr et al. 2022; Rasmussen et al. 2022).

1.1. The Central Nervous System: Constraints and Adaptations

Brains and spinal cords operate under severe constraints that have profound effects on fluid flow and mass transport. First, neural tissue is hungry. The human brain accounts for 2% of a person's mass but fully 20% of her energy use (Peng et al. 2014). Few organs come close to matching the brain's metabolic rate per gram (although the liver is a notable exception). Second, neural tissue lacks storage. Elsewhere in the body, nearby fatty tissue allows active cells to bank energy when they have a surplus and retrieve it when they have a shortfall. Having no fatty reserves, tissues in the brain and spinal cord require that nutrients be provided and waste removed in precise agreement with rates of uptake and output, respectively. Transport and flow must vary accordingly. Third, the central nervous system is sequestered from the bloodstream. Although blood vessels form a dense network that permeates brain tissue, with capillaries typically separated by just 250 μm , cranial blood vessels are sealed by tight junctions that prevent or inhibit large molecules from crossing the BBB. The BBB powerfully protects the brain from pathogens but eliminates an advective fluid and solute transport path that benefits other parts of the body, where large nutrient molecules and water are delivered through gaps in leaky blood vessels (Johnston & Papaiconomou 2002). Fourth, brain and spinal tissues have no lymph vessels. In other tissues, excess fluid in the extracellular space (ECS) is collected and returned to the bloodstream by the lymphatic system (Moore & Bertram 2018). However, lymph vessels extend inward only as far as the outer edge of the skull (Louveau et al. 2015, Aspelund et al. 2015, Mesquita et al. 2018, Ahn et al. 2019), so fluids and solutes must take a different exit path from deep brain tissue. Finally, brain tissue is boxed in. The rigid skull provides essential protection from impacts, but it also prevents the cranial compartment from growing or shrinking in response to the brain's needs. Cranial blood volume cannot increase or decrease without a simultaneous and reciprocal change in the volume of some other brain substance, usually CSF/ISF. The converse is true for cranial CSF/ISF volume, and implications for transport and flow are far-reaching. Much about the structure and operation of the central nervous system—especially its fluid transport systems—can be understood as adaptations to these constraints.

Most broadly, given its demand for nutrient supply and waste removal at rapid rates that are constantly modulated, the brain needs a second fluid and solute transport system in addition to the cardiovascular system. Since lymph vessels are absent from deep brain tissue and blood is isolated by the BBB, neither can satisfy this need entirely. It has long been suggested that the water-like CSF and ISF that surround and permeate the brain might participate in such a system, and some experimental evidence supports this idea. Finding the rate of evacuation of tracer (dye) from the brain to be nearly independent of the tracer's diffusivity, Cserr et al. (1981) pointed out that advective transport via flowing CSF could explain the observation, but diffusion alone could not. Wielding two-photon microscopes unavailable at the time of Cserr's experiments, Iliff et al. (2012) found that tracers injected into CSF were swept into the annular perivascular spaces (PVs) surrounding penetrating arteries, entered the brain ECS, and accumulated around veins. Among the tracers transported was amyloid beta, a waste protein whose accumulation correlates with Alzheimer's disease. Based on their observations, Iliff et al. (2012) proposed a closed-loop transport system in which fluid from outside the brain passes in via periarterial spaces, through ECS in deep brain tissue, and back out via perivenous spaces, suggesting it could play an important role in waste clearance.

Glial cells can be seen as another adaptation to the severe constraints under which the central nervous system must operate. Glia carry no nerve impulses but instead support the neurons that do, partly by breaking down metabolic wastes in place, reducing the need for transport. Glia also facilitate transport. One group of glial cells, the astrocytes, form the outer boundaries of the PVs with appendages called endfeet. Their cell membranes are densely decorated with aquaporin-4 (AQP4) water pores, which allow water molecules to cross membranes easily (aquaporins are not pumps and do not consume energy; they merely allow for rapid osmosis). Knocking out the *Aqp4* gene in mice, or even just preventing AQP4 from forming preferentially on endfeet, significantly hinders solute transport by brain CSF/ISF (Iliff et al. 2012, Xie et al. 2013, Mestre et al. 2018a). This fact led Nedergaard, Iliff, and collaborators to name the brain's CSF/ISF transport system the glymphatic system, as it is regulated by glia and plays a role analogous to the lymphatic system elsewhere in the body. For more information about the glymphatic system readers are referred to Nedergaard (2013), Jessen et al. (2015), Plog & Nedergaard (2018), Nedergaard & Goldman (2020), Hablitz & Nedergaard (2021a,b), and Rasmussen et al. (2022).

Another striking fact about the glymphatic system, which may also be an adaptation to constraints on the brain, is that CSF/ISF circulation deep in the brain occurs only during sleep and sleep-like states. Working with mice, Xie et al. (2013) showed that during natural sleep or sleep-like anesthetic states, compared to waking states, brain ECS grew 60%, inflow of tracer increased by more than an order of magnitude, and naturally occurring amyloid beta was evacuated from brain tissue more rapidly. In human brains, tracer evacuation occurs primarily during sleep and along similar pathways (Eide et al. 2021), with particularly strong CSF flows measured during non-rapid eye movement sleep (a deep-sleep phase) (Fultz et al. 2019). Beyond the instantaneous sleep/wake state, circadian rhythms also play an important role: Hablitz et al. (2020) found that transport due to CSF circulation in anesthetized mice was greater when the mice would typically have been asleep than it was when they would typically have been awake. Accordingly, it has been suggested that glymphatic function may be an essential reason that all animals, including humans, need to sleep; the enlarged ECS and increased flows that facilitate fluid and solute transport may interfere with neuronal activity to the point of being incompatible with consciousness. Additionally, glymphatic function has been observed not only in mice but also in rats (Ratner et al. 2017), pigs (Bèchet et al. 2021), alligators (Young et al. 2021), and humans (Eide et al. 2021).

Several features of the glymphatic system are still not well understood or are debated, including the driving mechanisms for perivascular flow of CSF, the existence of flow of ISF in the brain

Perivascular spaces (PVs): annular spaces surrounding blood vessels in the brain, bounded by astrocyte endfeet in cortical tissue or leptomeningeal tissue on the brain surface, often denoted as periarterial or perivenous

Amyloid beta: metabolic waste protein whose accumulation in brain tissue is common in Alzheimer's disease

Glial cells: cells in the nervous system that do not produce electrical impulses, but play a supporting role for neurons

Astrocytes: type of glial cell, named for their star-like shape, whose endfeet form the outer boundaries of penetrating PVs and are dense with AQP4

Endfeet: bulbous projections of cells, often at the end of narrow stalks

Aquaporin-4 (AQP4): protein embedded in cell membranes allowing rapid, passive transport of water molecules into/out of cells

parenchyma, and the role of AQP4 channels in the exchange of CSF and ISF; these and other issues are discussed in recent reviews (Ray et al. 2019, Mestre et al. 2020b, Bohr et al. 2022).

Glymphatic system: the brain's fluid and solute transport system, whose major pathways are organized along blood vessels or nerve sheaths and whose function is facilitated by AQP4

1.2. Implications of Cerebrospinal Flow for Human Health

Emerging knowledge of CSF flow and its role as a transport system in the central nervous system has important implications for human health. First, many neurodegenerative disorders correlate with and are thought to be caused by unhealthy accumulation of natural waste proteins, including Alzheimer's disease (amyloid beta and tau), Parkinson's disease (alpha-synuclein), and cerebral amyloid angiopathy (amyloid beta) (Nedergaard & Goldman 2020). Impaired or degraded CSF flow may contribute, particularly because waste clearance becomes impaired with age (Kress et al. 2014, Benveniste et al. 2019). Second, CSF flow is a key contributor to tissue damage during stroke and cardiac arrest. In both, tissue damage occurs largely because of local swelling (edema), presumably displacing fluid from elsewhere in the rigid skull, and for the first few minutes after a stroke or heart attack, the primary source of swelling is not blood but rather CSF rushing through PVs, driven by violent artery constrictions (Mestre et al. 2020a, Du et al. 2021). Third, an unhealthy accumulation of CSF in the skull, known as hydrocephalus, can result in headaches, double vision, and mental impairment. Its causes include Chiari malformation (displacement of tissue in the cerebellum at the base of the brain) and blockage of a narrow passage between brain ventricles (the cerebral aqueduct; see **Figure 1**), either of which prevents healthy CSF flow. Fourth, the formation of a cyst in the spinal cord, known as syringomyelia, impedes CSF flow there and can cause serious nerve damage. Finally, a fluid and solute transport system with direct access to the central nervous system is important for physiological delivery of nutrients and holds great promise for

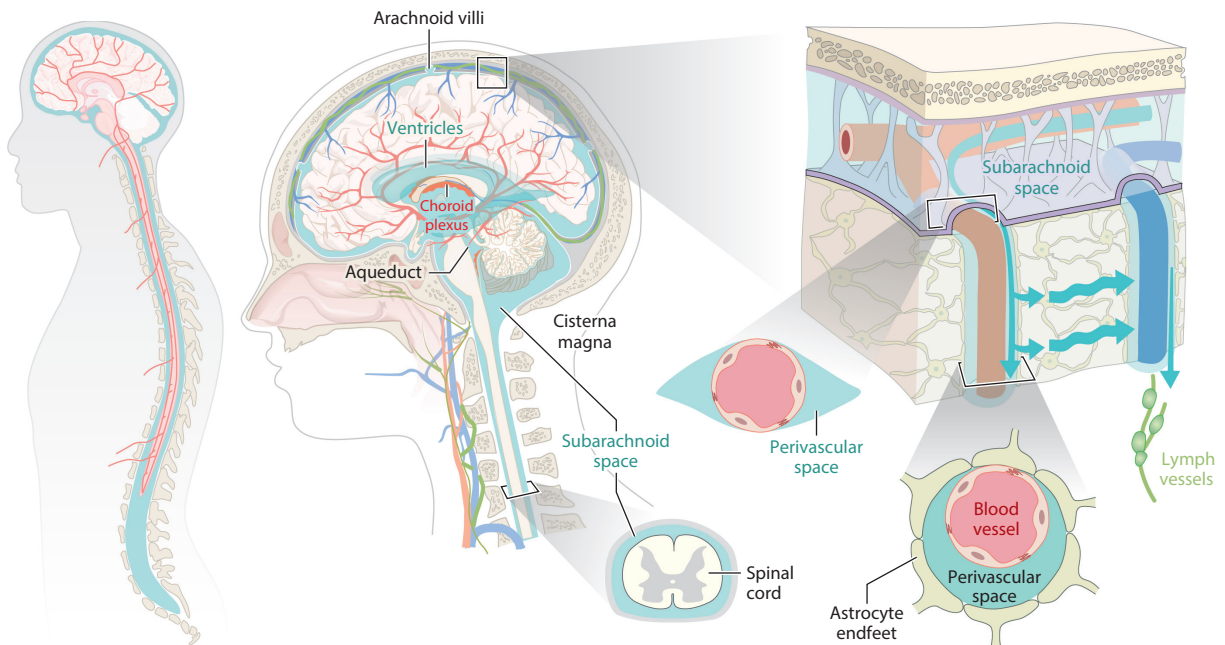


Figure 1

The anatomy of cerebrospinal and interstitial fluid circulation in the central nervous system. Large chambers, such as the ventricles and subarachnoid space, are contiguous with small chambers that penetrate brain tissue, such as perivascular spaces and nerve sheaths, allowing for global circulation and solute transport. In some chambers, fluid flows freely; in others, it moves slowly through porous media. Illustration by Dan Xue.

drug delivery, since it sidesteps the BBB, which allows only a small fraction of the blood-borne concentration of most drugs to enter brain tissue (Linninger et al. 2008, Tangen et al. 2015, Plog et al. 2018, Lilius et al. 2019, Kelley 2021).

2. ANATOMY OF FLUID PATHWAYS

The central nervous system is immersed in and permeated by water-like fluids, as sketched in **Figure 1**. Fluid provides the brain with mechanical isolation from the skull, thereby protecting brain tissue from injury. Fluid also flows. CSF is secreted from the choroid plexus, a branching network of cells and tissue that border the ventricles near the center of the brain. CSF is taken up by lymph vessels and perhaps by arachnoid granulations (Johnston & Papaiconomou 2002), both of which are near the skull. A long flow pathway is implied. From the lateral ventricles, CSF must pass to the third ventricle, then to the fourth via a narrow (~ 1 mm in humans) channel called the aqueduct of Sylvius, and then to the subarachnoid space. Lined with carpets of cilia, the ventricles are much larger than most other fluid spaces in the central nervous system. Ventricles may also connect directly to PVSs (Magdoom et al. 2019).

Positioned between brain tissue and the skull, the cranial subarachnoid space is primarily open but spanned intermittently by connective tissue and blood vessels. A wide region at the base of the back of the brain, the cisterna magna, is convenient for injecting tracer dye or particles during experiments. Some CSF from the subarachnoid space passes deep into the brain along periarterial spaces, then through the ECS within the tissue (probably quite slowly), and then out along perivenous spaces and white matter nerve tracts. The nature of flow in tissue and the precise routes out of the brain are topics of ongoing study. Substantial amounts of CSF may be secreted across the BBB (Petitelerc et al. 2021), in addition to what is secreted by the choroid plexus. Some CSF from the cranial subarachnoid space passes through the foramen magnum (one of the few openings in the rigid skull) to the spinal subarachnoid space and onward to lymphatic vessels there, and some CSF exits the cranium to the nose or to cervical lymph vessels (Johnston & Papaiconomou 2002; Ma et al. 2017, 2019). Many aspects of these complex flow pathways are topics of ongoing study. For example, because fluid flowing out of brain tissue carries away metabolic wastes, we might expect it to be anatomically separated in the subarachnoid space from the cleaner fluid that has not yet passed through brain tissue, but no such separation has been found. However, other anatomical aspects of the pathways are well known, and below we describe those relevant to fluid mechanics, particularly in PVSs and in the ECS within brain tissue.

2.1. Perivascular Spaces in the Brain

PVSs (sometimes also called paravascular spaces) are annular channels that surround the blood vessels throughout the brain and are filled with CSF (Wardlaw et al. 2020). The inner wall of a PVS is formed by the outer layer of the blood vessel. The outer wall of a PVS is formed by the endfeet of astrocytes, and gaps at the junctions of these endfeet permit the passage of fluid and large molecules. PVSs are generally much larger than the ECS in the parenchyma, which have widths occasionally reaching $1 \mu\text{m}$ but usually much less (Tønnesen et al. 2018, Paviolo et al. 2020) and, hence, have much lower hydraulic resistance. It is important to measure the size of PVSs *in vivo* because they shrink substantially upon fixation. The PVSs surrounding surface (pial) arteries in the mouse brain are about $20\text{--}40 \mu\text{m}$ wide (Iliff et al. 2012, Mestre et al. 2018b), but PVSs around smaller blood vessels in the parenchyma are correspondingly smaller, and PVSs surrounding the largest surface arteries in the human brain are correspondingly larger (Bedussi et al. 2018, Vinje et al. 2021).

Particle-tracking experiments have shown that the PVSs surrounding surface arteries in the mouse brain are open (nonporous) spaces (Min Rivas et al. 2020): This was established on the basis of the observed particle tracks, which show almost no tortuosity, and the mean velocity profiles, which compare well with theoretical profiles based on the Navier–Stokes equation. However, PVSs surrounding other blood vessels in the brain (penetrating arterioles, venules, and veins) likely contain a significant amount of connective tissue and other cells, and as such they are more appropriately treated as porous media. For a porous annular channel, for which the Darcy law applies, the hydraulic resistance for a fixed cross-sectional area is the same no matter the shape of the cross section. This contrasts with an open annulus, where changing the shape alters the hydraulic resistance, and for a given area there is an optimal shape that produces the least hydraulic resistance (Tithof et al. 2019). The hydraulic resistance of PVSs is discussed further in Section 4.2.

Wang et al. (2021) visualized astrocyte endfoot junctions throughout the mouse-brain vasculature using immunofluorescent labeling. They found that the endfoot size is positively correlated with blood vessel diameter, with larger blood vessels having larger endfeet and fewer gaps than smaller blood vessels. Based on a computational model, they found that this varying endfoot dimension produces a nearly uniform flux of fluid from PVSs into the ECS throughout the vascular network, and they suggested that this might be an evolutionary adaptation to maintain CSF-ISF exchange through deep brain structures.

Tracer studies reveal that there may be a continuous pathway of PVSs in the parenchyma, from arterioles through to veins, providing a low-resistance route for CSF flow (Rennels et al. 1985, Halnes et al. 2013, Hannocks et al. 2018, Pizzo et al. 2018). Such a route suggests the possibility that there is no flow of ISF within the ECS, but instead solutes are transported purely by diffusion to nearby PVSs, cross their outer walls, and are then transported out of the brain by the flow of CSF that runs through the network of PVSs (Thomas 2019). However, other studies have found no evidence of the capillary PVSs that would provide a continuous pathway (Lam et al. 2017), and substantial evidence supports slow flow of ISF within the ECS, as discussed in Section 5 below.

2.2. The Extracellular Space in the Brain

Tissues throughout the brain parenchyma require fluid transport in order to deliver nutrients and eliminate waste. This transport occurs in the ECS that surrounds all the cells in the parenchyma and is filled with ISF, which has a composition very much like that of CSF. The extent of the ECS can be described by its volume fraction $\alpha \equiv V_{\text{ECS}}/V_{\text{TOTAL}}$: this volume fraction is about 20% in anesthetized mice. The volume fraction α can change significantly in response to brain activity over a range of timescales: over a day (sleep–wake cycle; Xie et al. 2013), over minutes (spreading depolarization; Hrabě & Hrabětová 2019), or over seconds (epilepsy; Colbourn et al. 2021).

Nicholson & Hrabětová (2017) have provided a thorough review of the properties of the ECS. More recently, super-resolution fluorescence microscopy has provided more details of the structure of the ECS (Tønnesen et al. 2018, Paviolo et al. 2020). The widths of individual ECSs in the mouse brain are highly variable, ranging from less than 50 nm to more than 1 μm .

In fluid dynamics modeling, brain tissue is usually treated as a porous medium, with porosity equal to the volume fraction α , and the flow is described by the Darcy law (see Section 5).

3. METHODS

Both experimental and numerical methods have made major contributions to current understanding of CSF flow and are rapidly advancing. As in many fields, breakthroughs in methods have frequently revealed new information and heralded breakthroughs in knowledge. In experiments, the flow of CSF itself and the transport of solutes dissolved in CSF are typically entangled, since

detecting CSF motion without solutes as tracers is rarely (but sometimes) possible. In simulations, flow and transport are typically entangled because both processes are important to scientific questions and clinical applications.

3.1. Experimental Methods

Understanding the fluid mechanics of water-like flows in the central nervous system requires information about many quantities, including fluid properties, boundary shapes, solute transport rates, flow velocities, pressure gradients, and tissue properties. Experiments can provide key information. The properties of fluids in the central nervous system are simpler than those of many biological systems: CSF and ISF have low protein content and are well modeled as water, Newtonian, and incompressible (Bloomfield et al. 1998).

Shapes and sizes of fluid boundaries in the central nervous system are often measured *in vivo* because of the many known and unknown changes imposed on tissue during death and fixation (Ma et al. 2019; Mestre et al. 2018b, 2020a). Magnetic resonance imaging (MRI) (Ratner et al. 2017, Fultz et al. 2019, Benveniste et al. 2020, Eide et al. 2021, Stanton et al. 2021) produces 3D images of whole brains, spines, or bodies and requires no surgery but achieves relatively low resolution ($\sim 10^2$ or $10^3 \mu\text{m}$; $\sim 0.1\text{--}10$ Hz). Two-photon imaging (Bedussi et al. 2018, Mestre et al. 2018b) produces 3D images, can penetrate $\sim 400 \mu\text{m}$ deep (spanning much of the mouse cortex), and has excellent resolution (submicron; $\sim 10^2$ Hz in two dimensions), but requires tracer injection and invasive surgery. Imaging through intact mouse skulls using a standard microscope (Plog et al. 2018) has good resolution ($\sim 1 \mu\text{m}$; $\sim 10^2$ Hz or more) but produces 2D projections of 3D anatomy and is invasive. Once images are gathered, segmenting boundaries from fluid spaces can be surprisingly tricky; future work might improve existing methods.

Transport of tracer dyes and some endogenous solutes can be measured directly via MRI, two-photon imaging, or standard optical microscopy. For those methods, solute concentrations are typically assumed to be proportional to image brightness, but calibration is difficult, not least because many tracers are produced and broken down by the body. Positron emission tomography and single-photon computed tomography use radioactive tracers that remain detectable even if metabolized, allowing for robust calibration, but they have lower resolution than MRI and require tracer injection.

Flow velocities in surface PVSs can be measured via tracking of fluorescent particles, usually with two-photon or standard optical microscopy (Bedussi et al. 2018, Mestre et al. 2018b, Raghunandan et al. 2021). Particles do not enter penetrating PVSs, however. MRI can track the motion of water molecules, but current methods fit that motion to a tensorial diffusivity, not to a velocity. New MRI methods quantify water displacement (Fultz et al. 2019) and might be used to produce velocity measurements. Alternately, fluid velocity can be estimated from the measured motion of tracer dyes. If regions of high and low concentration are separated by sharp fronts, automated front-tracking (Plog et al. 2018) can estimate fluid velocity, although this technique neglects diffusion and is therefore accurate only when the Péclet number (see Section 7) is large. Data-driven methods (Ratner et al. 2017, Koundal et al. 2020, Valnes et al. 2020, Ray et al. 2021, Chen et al. 2022) infer velocity by combining measured tracer motion with the known equations of solute transport. The potential for quantitative, high-resolution, noninvasive flow measurements make data-driven methods an important topic for ongoing work.

Pressure can be measured only at isolated points by inserting probes, making intracranial pressure gradients all but unknown. Few studies have measured intracranial pressure at even two points simultaneously (Eide et al. 2012, Young et al. 2021); none has done more. Data-driven methods might estimate pressure in future work.

Functional

hyperemia: local, temporary increase in blood flow to active brain regions, achieved by artery dilation that displaces CSF

Tissue properties relevant to fluid mechanics include porosity, tortuosity, and permeability of brain tissue (which is often modeled as a porous medium; see Section 5), as well as the elasticity of all tissues that bound fluid spaces. Porosity and tortuosity can be measured via real-time iontophoresis (Nicholson & Phillips 1981) or integrative optical imaging (Nicholson & Tao 1993), in which tissue is injected with a tracer whose spread over time is fit to an analytic solution of the diffusion equation. Imaging thin tissue slices with an optical or electron microscope can produce 3D images of the ECS. Simulating flow through those spaces (Holter et al. 2017) or through a geometric approximation (Jin et al. 2016) allows one to calculate porosity, tortuosity, and permeability, but tissue fixation changes ECS size and shape significantly. Super-resolution techniques like stimulated emission depletion microscopy require fixation techniques that are less disruptive than electron microscopy while achieving excellent spatial resolution (~ 10 nm) (Nägerl et al. 2008, Godin et al. 2017), but they cannot yet be used *in vivo*. By definition, measurements made in a living organism are most faithful to the physiology. That said, *in vitro* experiments can offer not only better resolution and sensitivity but also more powerful control and a greater ability to test fluid mechanical hypotheses. Future studies may rely more heavily on *in vitro* methods, perhaps combining controlled flows driven by microfluidic devices with cells or tissue samples that preserve some of the physiological biochemistry.

3.2. Numerical Methods

Numerical methods for modeling CSF flow are rapidly advancing and diversifying. The Reynolds number is small for most CSF flows. Defined as $Re = U\ell/\nu \sim 10^{-3}$, where ν is the kinematic viscosity and ℓ is the length scale of the cross section, it is small in surface PVSs (Mestre et al. 2018b), lower still in penetrating PVSs and ECSs (because they are smaller and carry slower flow), and presumably higher in the (larger) subarachnoid space. Thus, inertial effects are highly unlikely. Considering the spinal column, Sánchez et al. (2018) defined Re in terms of the Womersley number and found that, although Re is much less than 1, accurate modeling of long-term transport requires including steady streaming (a nonlinear effect).

Though CSF is simple in that it can be modeled accurately as water, other circumstances make simulation challenging. The tortuous microscale passageways of the ECS are far too complicated to consider in full detail over large regions; fortunately, brain tissue can be accurately modeled as a porous medium. Larger anatomical structures cannot, despite having boundary shapes that are nearly as complicated. Worse, boundaries deform, and their deformation is subject to mechanisms spanning a wide range of characteristic timescales, including the cardiac cycle ($\sim 10^0$ Hz), the respiratory cycle ($\sim 10^{-1}$ Hz), and functional hyperemia (low-frequency variations in local cortical blood volume, $\sim 10^{-2}$ Hz). Boundary motion drives CSF flow, and boundaries may be soft enough that CSF flow in turn deforms them [cf. Kedarsetti et al. (2020a), although further measurements are needed]. Perivascular networks are vast, spanning nine or more generations of bifurcations in the mouse brain (Blinder et al. 2010, Tithof et al. 2022) and significantly more in the larger human brain. Surface perivascular networks are also likely to include loops (anastomoses), given that surface arterial networks do (Blinder et al. 2010).

Augmenting CSF flow simulations with solute transport simulations introduces additional complexities. Characteristic times for advection and diffusion often differ by orders of magnitude, introducing additional timescales into the problem and making it notoriously expensive to simulate (the ratio of timescales is quantified by the Péclet number; see Section 7). Considering all these challenges, fully resolved, 3D simulations of CSF flow through the entire central nervous system lie well beyond current computational capabilities. Aside from computational cost, uncertainties in material parameters and boundary conditions would make the accuracy and relevance of such simulations questionable.

Nonetheless, great progress has been made both by high-fidelity simulations of small parts of the CSF circulation system and by lower-fidelity simulations spanning much of the system in order to capture interactions among parts. First, consider high-fidelity simulations. Where tissue can be modeled as a porous medium, researchers have used Darcy's law (Equation 3) (Asgari et al. 2015, Schreder et al. 2022) or the Darcy–Brinkmann equation (Sharp et al. 2019). Useful numerical schemes include the superposition of analytic solutions (Schreder et al. 2022) and finite-element methods. One recent study modeled brain tissue as poroelastic and solved via a finite-element scheme (Kedarasetti et al. 2021). Where CSF passes through open spaces, researchers have used the Stokes equation, or sometimes the more general Navier–Stokes equation (although its additional, nonlinear term is usually negligible for $Re \ll 1$). Analytic models have employed lubrication theory in order to make exact predictions in simplified domains (Bilston et al. 2003, Schley et al. 2006, Wang & Olbricht 2011). Solving the Navier–Stokes equation in two dimensions enabled a study of the effects of PVS cross-sectional shape on hydraulic resistance (Tithof et al. 2019). Useful numerical schemes include finite-element methods, immersed boundary methods, and lattice Boltzmann methods, all of which accommodate complicated boundary shapes. When boundaries are soft and two-way fluid–structure interaction is to be considered, either finite elements with arbitrary Lagrangian–Eulerian coordinates or lattice Boltzmann methods are most common. Simulations of solute transport have used finite-difference (Troyetsky et al. 2021) and finite-element (Vinje et al. 2021) methods.

Numerical methods for simulating blood flow are more mature and can sometimes be adapted to CSF flow, but complications arise. The Reynolds number for blood flow is significantly higher than that of CSF ($\sim 10^2$ in some places), and hypothesized CSF flow mechanisms like perivascular pumping involve length scales and timescales not readily accommodated by established packages for simulating blood flow (e.g., SimVascular). Because parts of the CSF circulation system are soft, the accuracy of local simulations is improved when system-wide hydraulic resistance (accounting for viscous resistance to flow, analogous to electrical resistance; see Equation 1) and compliance (accounting for boundary elasticity, analogous to electrical capacitance) are included in the inlet or outlet boundary condition (de Guevara et al. 2022), as has long been done for blood flow simulations.

Next, consider lower-fidelity simulations that span more of the CSF circulation system in order to capture interactions among its parts. By averaging radially and azimuthally, the flow equations in line-like CSF passageways (e.g., PVSs) can be reduced to a 1D form that captures much of the 3D nature of the flow with far lower computational cost (Gjerde & Rognes 2021, Daversin-Catty et al. 2021, Sincomb et al. 2022). 1D models (also common in blood flow simulations) can therefore accommodate domains that include large perivascular networks, with bifurcations and loops. Even simpler than a 1D model is a lumped-parameter model, sometimes described as zero-dimensional, in which each CSF passageway is characterized by a hydraulic resistance and perhaps also a compliance. Hydraulic network models (Asgari et al. 2015, Faghieh & Sharp 2018, Rey & Sarntinoranont 2018, Mestre et al. 2020a, Du et al. 2021, Boster et al. 2022, Tithof et al. 2022) can be solved with simple matrix-inversion methods developed for electrical circuits and are so cheap that they can conveniently be repeated many times, with varying parameters and initial conditions, allowing for Monte Carlo experiments. Control volume models, which focus on fluid exchange among specified regions of the CSF circulation system (Linninger et al. 2008, Vardakis et al. 2020, Vinje et al. 2020, Elbert et al. 2022), are built by casting the equations of fluid mechanics in integral (not differential) form, can be solved with less-detailed knowledge of boundary shapes, and make predictions that are readily comparable to many *in vivo* observations. Tremendous promise lies in multiscale coupling of system-wide, lower-fidelity simulations with local, high-fidelity simulations.

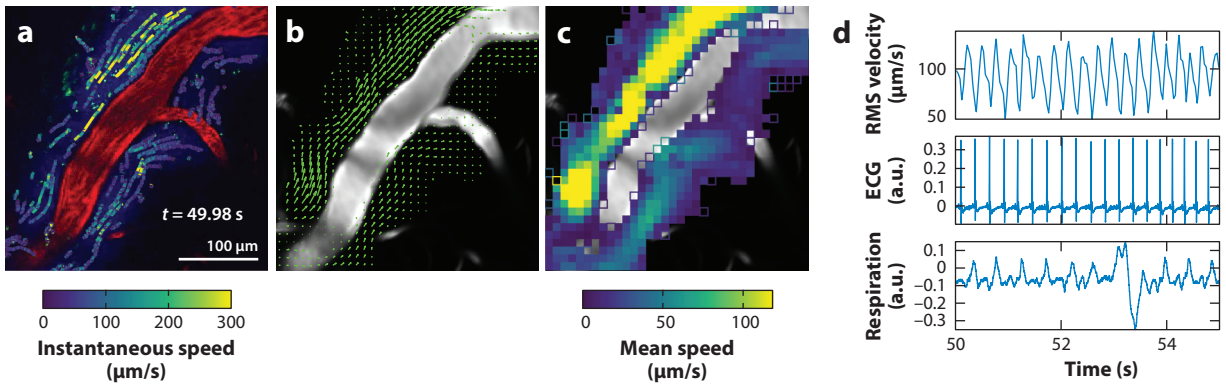


Figure 2

Measuring flow in the surface perivascular space of a live mouse via particle-tracking. (a) Micron-scale fluorescent tracer particles (green) injected at the back of the skull are swept along by flowing cerebrospinal fluid (CSF) (blue) and pass through the perivascular space surrounding a surface artery (red). Automated particle-tracking measurements of tracer particles' positions and velocities make it possible to overlay pathlines colored according to the instantaneous velocity of each. (b,c) Averaging many such measurements over time results in a mean flow field. Solid squares indicate regions where ≥ 15 measurements were made; open squares indicate regions where < 15 measurements were made (see also **Supplemental Video 1**). (d) The instantaneous root-mean-square (RMS) CSF velocity pulses in synchrony with the cardiac cycle [as determined by electrocardiogram (ECG)] and shows little correlation with the respiratory cycle. Imaging provided by A. Ladrón-de-Guevara and M. Nedergaard; analysis by Y. Gan and D.H. Kelley.

4. FLOW IN PERIVASCULAR SPACES

4.1. Experimental Measurements

Beginning with the pioneering work of Helen Cserr in the 1970s, many experiments have produced evidence that bulk flow of CSF occurs in PVSs throughout the brain (Cserr et al. 1977, 1981; Szentistványi et al. 1984; Rennels et al. 1985; Ichimura et al. 1991; Abbott 2004; Hadaczek et al. 2006). Recent *in vivo* experiments with mice revealed CSF flow in PVSs around surface arteries, with net (bulk) flow in the direction of the blood flow and pulsation synchronized with the cardiac cycle (Bedussi et al. 2018, Mestre et al. 2018b). Measurements from one such experiment are shown in **Figure 2**. Using particle-tracking in surface PVSs, Mestre et al. (2018b) found that the artery wall velocity closely matched CSF flow velocity, and that altering the artery wall motion by raising the blood pressure to cause arterial stiffening significantly reduced the net flow rate, suggesting that artery wall motion at the cardiac rate is an important driver. Earlier, Iliff et al. (2013) altered the pulsation of mouse carotid arteries (50% decrease by surgery and 60% increase by dobutamine), finding that CSF-ISF exchange varied accordingly and concluding that arterial pulsatility is a key driver of CSF flow in the brain.

There has been controversy about the direction of CSF flow along PVSs. Considering images of tracer in fixed tissue, Weller and colleagues proposed that periarterial spaces serve as routes for outflow, with net flow in the direction opposite that of blood flow, and that this reverse flow occurs not in the PVS but in the basement membrane of the smooth muscle cells that surround the artery (Carare et al. 2008, Albargothy et al. 2018). Simulations (Coloma et al. 2016) and fluid mechanical experiments (Coloma et al. 2019) have demonstrated that reverse flow is possible in principle if traveling waves on artery walls are reflected [the mechanism is essentially impedance pumping (Hickerson & Gharib 2006, Avrahami & Gharib 2008)]. An extensive discussion of this controversy is given by Bohr et al. (2022). Here we only point out that *in vivo* particle-tracking experiments (Bedussi et al. 2018, Mestre et al. 2018b, Raghunandan et al. 2021) show that net

Supplemental Material >

flows in surface PVSs are hardly ever antiparallel to the blood flow. If antiparallel flow were to occur in basement membranes, their 100-nm size (Sharp et al. 2019) would imply (via Poiseuille's law) volume flow rates smaller than those in the 40- μm PVS by a factor of roughly 10^8 , making it altogether negligible.

4.2. Hydraulic Resistance of Perivascular Spaces

For steady flow along a uniform vessel, the volume flow rate Q is proportional to the pressure gradient dp/dz along the vessel. The inverse of that proportionality constant is the hydraulic resistance \mathcal{R} (per unit length), according to the hydraulic analog of Ohm's law:

$$Q = \frac{-dp/dz}{\mathcal{R}}. \quad 1.$$

Hydraulic resistance impedes a flow driven by a pressure drop and is therefore analogous to electrical resistance, which impedes a current driven by a voltage drop. In the case of steady Poiseuille flow in an open (nonporous), straight, uniform annular vessel, the full axial velocity profile $u(x, y)$ can be determined for a specific shape and area of the cross section. The z -component of the Navier–Stokes equation reduces to the Poisson equation,

$$\frac{\partial^2 u}{\partial x^2} + \frac{\partial^2 u}{\partial y^2} = \frac{1}{\mu} \frac{dp}{dz}, \quad 2.$$

where μ is the dynamic viscosity and the pressure gradient dp/dz is constant and negative (for flow in the positive z -direction). Computing the solution, subject to the no-slip condition $u = 0$ at the walls, is straightforward, and the volume flow rate Q and the corresponding hydraulic resistance \mathcal{R} can be obtained from the computed velocity profile.

Modeling CSF flow in PVSs requires knowing their sizes and shapes. Measurements *in vivo* show that the cross section of periarterial spaces is usually not a concentric circular annulus: Instead, the outer boundary is often flattened in the direction perpendicular to the skull and eccentric with respect to the artery, as shown in **Figure 3**. Tithof et al. (2019) presented an adjustable geometric model to approximate these shapes using a circular artery and an elliptical outer PVS wall. These two boundaries are allowed to be nonconcentric, and the radius of the inner circle, the semiaxes of the ellipse, and the eccentricity can be varied to produce different shapes that match actual cross sections quite well. With enough flattening, the outer wall can contact the artery, splitting the PVS into two disconnected regions, as observed *in vivo*.

The hydraulic resistance of any shape decreases sharply with increasing cross-sectional area, as expected from dimensional analysis. If the area of an eccentric circular annulus is held fixed, an analytic solution shows that hydraulic resistance decreases monotonically with increasing eccentricity (White 2006): Placing more fluid farther from the walls reduces the average shear stress and hence the hydraulic resistance, which can drop by a factor of 2.5 due to eccentricity alone. For the same reason, the hydraulic resistance of an elliptical annulus of fixed area is minimum when the elongation is moderate. With zero elongation, the outer boundary is circular, so no fluid is very far from the walls, but with extreme elongation, the ellipse itself is so narrow that no fluid is far from the wall. PVS shapes measured *in vivo* have near-minimum resistance, with corresponding eccentricity and elongation. Tithof et al. (2019) suggested that PVS shapes might be an evolutionary adaptation to permit more efficient clearance of metabolic wastes.

Vinje et al. (2021) computed hydraulic resistances numerically for realistic geometric models of PVSs around arteries and veins. The PVSs around veins, being smaller, had higher hydraulic resistance. The authors then claimed that volume flow rates are greater in periarterial spaces than

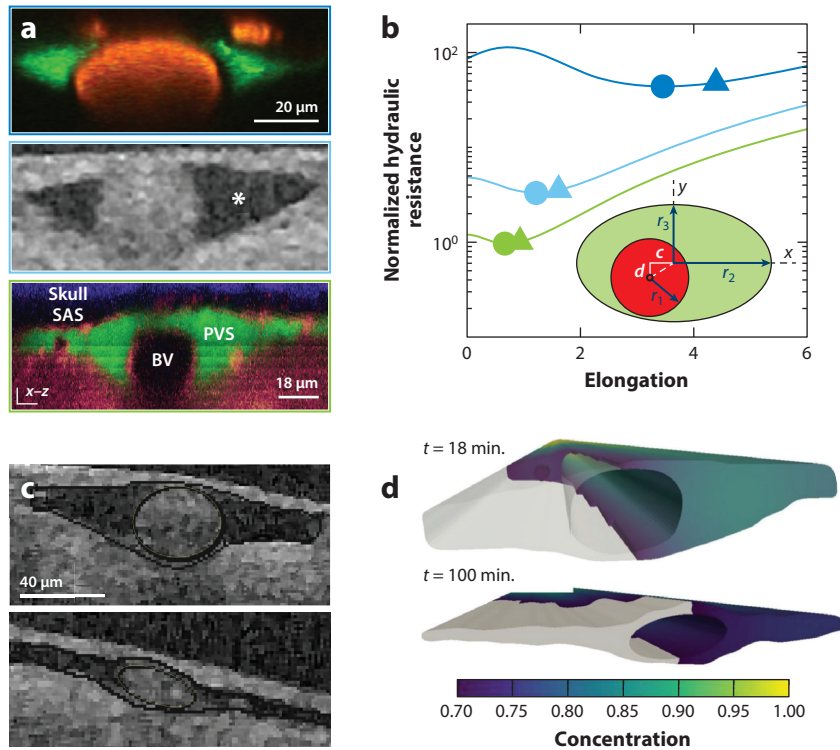


Figure 3

Shapes of surface PVSs. (a) In vivo images showing cross sections of surface PVSs in mouse (top, bottom) and human (middle). Images adapted with permission from (top) Mestre et al. (2018b) (CC BY 4.0); (middle) Bedussi et al. (2018) (CC BY-NC 4.0); and (bottom) Schain et al. (2017) (CC BY 4.0). (b) A simple model parameterizing cross-sectional shapes of PVSs with a circle and an ellipse allows the normalized hydraulic resistance for many such shapes to be calculated, revealing that resistance has minimum values (circles) at a particular elongation (with other parameters held constant) and that in vivo shapes have nearly the same elongation (triangles). Curve colors match border colors for the corresponding shapes in panel a. Panel adapted from Tithof et al. (2019) (CC BY 4.0). (c) In vivo images showing cross sections of human periarterial (top) and perivenous (bottom) spaces. (d) Advection–diffusion equations in domains built from in vivo images show that solute transport is faster in periarterial spaces than perivenous spaces, if the pressure drop is the same across each, because periarterial spaces are bigger. Panels c and d adapted from Vinje et al. (2021) (CC BY 4.0). Abbreviations: BV, blood vessel; PVS, perivascular space; SAS, subarachnoid space.

in perivenous spaces. That conclusion, however, depended on the questionable assumption that the pressure drop is the same in each case. Hydraulic network models (see Section 8) predict instead that pressure drops vary widely from place to place along CSF pathways.

The hydraulic resistances calculated for steady Poiseuille flow are also relevant for the observed pulsatile flows in PVSs. Viscous, incompressible, laminar flows in uniform vessels due to oscillating pressure gradients are well understood, and analytic solutions are known for some cross sections. The nature of the solution depends on the dynamic Reynolds number, $R_d = \omega \ell^2 / \nu$ (or, alternatively, the Womersley number, $\alpha = \sqrt{R_d}$), where ω is the angular frequency of the oscillating pressure gradient. For $R_d \ll 1$, as in the case of flows in PVSs [for example, for the mouse brain, with $\omega = 25.13 \text{ s}^{-1}$ (corresponding to a pulse rate of 240 bpm), $\ell = 20 \text{ }\mu\text{m}$ (typical width of a pial PVS), and $\nu = 7.0 \times 10^{-7} \text{ m}^2\text{s}$, we have $R_d = 1.4 \times 10^{-2}$], inertial effects are negligible and the

velocity profile is very nearly that of quasi-static Poiseuille flow in phase with the oscillating pressure gradient (White 2006, sections 3–4.2). For a pulsatile (oscillatory plus steady) flow, the average volume flow rate is inversely proportional to the same hydraulic resistance that applies to steady Poiseuille flow.

A PVS that contains a significant amount of connective tissue is not an open space and can be treated as a porous medium whose resistance can be calculated using Darcy's law. In this case the hydraulic resistance for a fixed cross-sectional area A_{pvs} is the same no matter what the shape of the cross section. The Darcy flux q is uniform over the cross section, so altering the shape will not change the volume flux rate $Q = A_{\text{pvs}}q$.

4.3. Driving Mechanisms

The mechanisms that drive the flow in PVSs are poorly understood, and several have been proposed. The pulsatile flow along arterial PVSs, with net flow in the same direction as the blood flow, has been attributed to peristaltic pumping by arterial pulsations, a mechanism known as perivascular pumping (Hadaczek et al. 2006). Peristalsis generally drives a pulsatile flow with both an oscillatory component and a steady component in the direction of the wall wave (Jaffrin & Shapiro 1971). Several theoretical studies have modeled this mechanism in a channel or annular tube with a radial-displacement wave traveling along the inner wall, representing the artery (Bilston et al. 2003, Schley et al. 2006, Wang & Olbricht 2011, Rey & Sarntinoranont 2018, Kedarasetti et al. 2020b, Carr et al. 2021, Yokoyama et al. 2021). Multiple models have predicted steady flow components with similar magnitudes to those observed in vivo but usually accompanied by a much stronger oscillatory component than is observed. Modeling end boundary conditions that account for the resistance and compliance of the rest of the CSF circulation system (Windkessel boundary conditions) brings closer agreement (de Guevara et al. 2022). Another source of disagreement is the wavelength of arterial pulsations, which at ~ 1 m is far greater than the length of a PVS segment (~ 250 μm) but is sometimes assigned a value similar to the length in order to simplify analytic reasoning and ease computational expense. Daversin-Catty et al. (2021) found that simulating domains whose lengths were shorter, compared to the wavelength, yielded less flow. A fully satisfactory model of the mechanisms that drive flow in PVSs has yet to be produced.

In flattened PVSs (see above), peristaltic pumping is predicted to produce azimuthal motions of the fluid in addition to axial and radial motions (Thomas 2019, Carr et al. 2021, Coenen et al. 2021). The pumping is stronger where the width of the channel is narrower, causing oscillating azimuthal pressure gradients that drive an oscillatory component of flow in the azimuthal direction.

Future studies should consider and evaluate the peristaltic pumping mechanism in light of improved end boundary conditions and realistic wavelengths. If peristaltic pumping cannot reproduce the observed steady flow component, the flow direction may be set by one or more other mechanisms. Only a small average pressure gradient (~ 1.5 mmHg/m) is required (Kedarasetti et al. 2020a, Daversin-Catty et al. 2021). Several authors have suggested that directed flow might be an artifact of the injection of tracer particles (Smith et al. 2017, Smith & Verkman 2018, Croci et al. 2019, Sharp et al. 2019, Kedarasetti et al. 2020a, Vinje et al. 2020, Faghieh & Sharp 2021), but subsequent experiments with no net injection of fluid produced flows that were statistically indistinguishable from those measured using typical injection methods (Raghunandan et al. 2021).

An alternate physiological mechanism for driving directed flow is functional hyperemia, the increase of blood flow to neurologically active brain regions: The associated vasodilation would squeeze fluid in the PVSs provided that the outer wall of the PVS remained relatively rigid (Kedarasetti et al. 2020b). van Veluw et al. (2020) used visual stimulation to induce functional hyperemia in awake mice, verifying that artery wall motion increased and finding that tracer was cleared more rapidly from PVSs. However, tracer was introduced through a local break in the

BBB, which may itself have driven flow. More broadly, this mechanism is essentially perivascular pumping on a longer timescale, and as such it faces similar difficulties in producing a directed flow. Moreover, functional hyperemia is likely not the only driving mechanism because flow along PVSs has been observed even when no sign of the low-frequency activity characteristic of functional hyperemia appeared in measurements of CSF flow speed, heart activity, or respiratory activity (Mestre et al. 2018b).

Kedarasetti et al. (2021) suggested another possible mechanism for directing flow: poroelasticity of the brain tissue surrounding PVSs. Using simulations, these authors found that if pressure pulses in PVSs not only drive fluid into the porous ECS but also cause the space to expand elastically, then the resulting nonlinearity causes more CSF to enter brain tissue than to leave it. Temporal asymmetry of pulse waveforms amplified the rectification effect. Assuming that CSF is neither created nor destroyed, directed flow into brain tissue from periarterial spaces requires a closed-loop circulation, with flow directed out of brain tissue elsewhere, as seen in experiments. However, this idea leads to a conundrum: Naively, we would expect poroelasticity to drive directed flow into brain tissue not only from periarterial spaces but also from all other open spaces, preventing any closed-loop circulation. That being said, pressure fluctuations may be different in other open spaces, and tissue poroelasticity may differ from place to place. Further study of poroelastic pumping is warranted.

5. FLOW OF INTERSTITIAL FLUID IN THE BRAIN EXTRACELLULAR SPACE

The current glymphatic model includes fluid exchange between the PVSs and the ECS and a slow flow of ISF in the parenchyma. There is substantial indirect evidence for such a flow. Croci et al. (2019) simulated combined diffusive and advective transport in the brain parenchyma following the injection of a tracer and found that diffusion alone cannot explain the distribution of tracer seen in the MRI study of Ringstad et al. (2017). Ray et al. (2019) found a better fit to the experimental data used to determine effective diffusion coefficients in brain tissue if a flow is included, with a speed up to 50 $\mu\text{m}/\text{min}$. Those authors went on to estimate the Péclet number in brain tissue, finding $6 \leq Pe \leq 18$ for gadoteridol dye (molecular mass 550 Da); Pe would be higher for larger molecules like amyloid beta. At this flow speed, advection would be the dominant transport mechanism for large molecules in the ECS (for which the Péclet number would be greater than unity). Estimating flow speeds from tracer motion via optimal mass transport suggests that both advection and diffusion contribute significantly to transport in the ECS (Koundal et al. 2020). A scale analysis of the basic equations (Thomas 2022) shows that the wake-to-sleep increase in porosity of the tissue (Xie et al. 2013) produces slightly decreased diffusive transport (because of dilution) but substantially increased advective transport (because of reduced hydraulic resistance), which would help explain the greatly increased solute clearance observed during sleep. This finding is consistent with earlier results from the detailed modeling of Jin et al. (2016). Beyond wake-to-sleep changes, Plog et al. (2018) found that dye entered brain tissue significantly faster after the tissue porosity was increased via the injection of hyperosmotic solutions. Given the scale analysis of Thomas (2022), that observation again supports the presence of advection in the ECS.

In fluid mechanical models, the brain parenchyma with its ECS is usually treated as a porous medium, and the flow of ISF is described by the Darcy law,

$$\mathbf{q} = -\frac{\kappa}{\mu} \nabla p, \quad 3.$$

where p is the pressure, κ is the permeability, μ is the dynamic viscosity, and \mathbf{q} is the superficial (Darcy) velocity, related to the actual (microscale) velocity by $\mathbf{u} = \mathbf{q}/\alpha$. The dependence of the

permeability κ on the porosity α and tortuosity λ is typically taken to be described by the Kozeny–Carman equation,

$$\kappa = \frac{\alpha^3}{\lambda \mathcal{A}^2 (1 - \alpha^2)}, \quad 4.$$

where \mathcal{A} is the specific surface area. For Darcy flow, the hydraulic resistance is inversely proportional to the permeability, which, for the brain parenchyma, is poorly quantified: Estimates of its value in the mouse brain span more than two orders of magnitude (Basser 1992, Holter et al. 2017). Low estimates of the permeability (high resistance) have been the basis for claims against any significant flow of ISF (Jin et al. 2016, Holter et al. 2017). Experimental methods for determining the effective diffusivity of molecules within the ECS are based on the assumption that there is no flow of the ISF and that transport is by diffusion alone (Nicholson & Hrabětová 2017).

Example studies of flow in the brain ECS are highlighted in **Figure 4**. Holter et al. (2017) presented such a model, based on flow from a single line source (arteriole PVS) to a single sink (venule PVS), using a porosity estimated from a geometric model of the ECS. They found the flow to be too slow to be significant in most cases (very low Péclet number). Ray et al. (2019) modeled Darcy flow between evenly spaced periarterial and perivenous spaces. Schreder et al. (2022) modeled ISF flow as a Darcy flow, driven by pressure drops in an array of parallel line sources (penetrating periarterial spaces) and line sinks (penetrating perivenous spaces). They calculated the effective hydraulic resistances for different arrangements of blood vessels based on imaging of mice and primates. Their results show the resistance varying significantly with vessel density and arteriole-to-venule ratio, both of which differ among species.

Flow from PVSs into the parenchyma has also been modeled. The endfoot gaps in the PVS walls provide a pathway for this flow. Romanò et al. (2020) modeled the PVS wall as permeable and elastic and used lubrication theory to calculate the flow driven across the wall by an imposed peristaltic deformation of the artery wall. Wang et al. (2021) found that the endfeet surrounding smaller vessels are themselves smaller, producing a greater gap length per unit interface area. They modeled flow through a network of PVSs and endfoot gaps, based on electron microscope images, and found that allowing for this variation in gap size produced a more uniform flow from PVSs to the parenchyma over the entire cerebrovascular tree.

6. FLOW OUTSIDE THE BRAIN

Beyond the small ECSs among brain cells, and beyond the PVSs and nerve sheaths that penetrate and wrap around the brain, CSF also flows through larger spaces in the central nervous system, including the subarachnoid space, brain ventricles, and spinal canal. Because these spaces are all contiguous, CSF motion in any one affects others, and all should be considered. Linninger et al. (2016) provided an excellent review of CSF flow in these spaces, so here we focus primarily on studies published more recently. A few examples are shown in **Figure 5**.

The human choroid plexus secretes ~ 1 L of CSF per day (Rasmussen et al. 2018), implying a slow net flow rate sometimes called the third circulation. But as discussed above, secretion is not the only driver of flow in these spaces. Brain tissue swells and shrinks as its blood content varies, with CSF exiting and reentering the skull accordingly. Oscillatory CSF flow occurs with each cardiac cycle, with respiration (inhalations increase brain blood content), and in response to varying demand for energy and oxygen (functional hyperemia). In vivo measurements usually show significantly faster flow at the cardiac frequency than at the respiratory frequency (Yildiz et al. 2017, Sincomb et al. 2020), and both of those oscillations drive flow faster than the steady flow driven by secretion. Although measurements of CSF flow in ventricles and subarachnoid spaces are difficult to make, Fultz et al. (2019) found that oscillating CSF displacement at the base

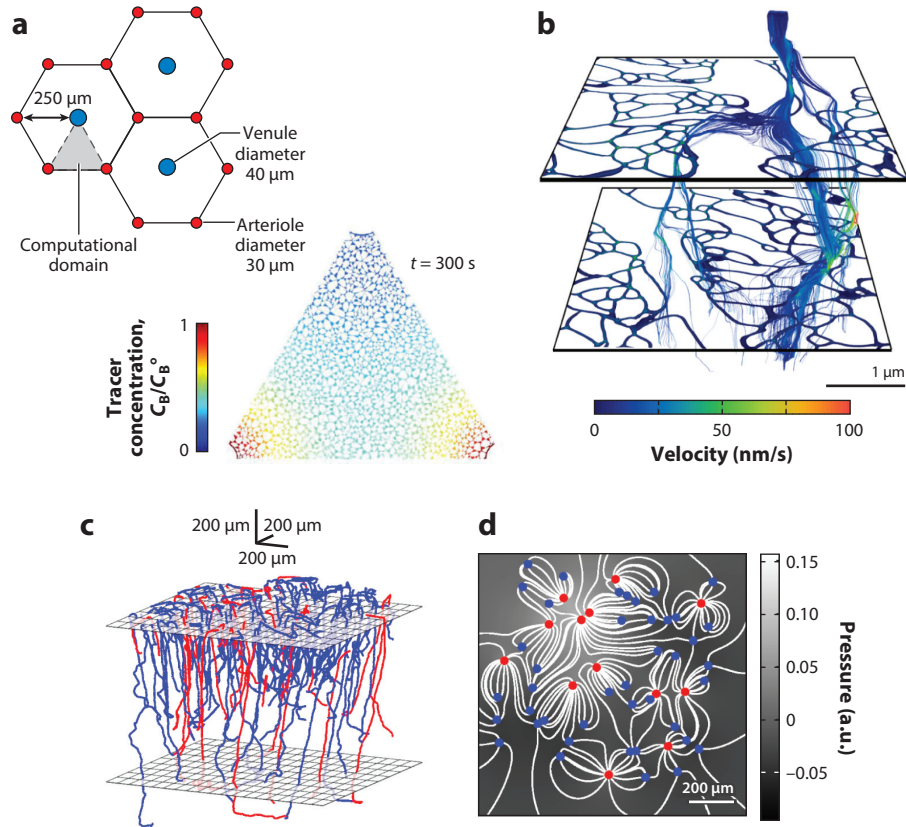


Figure 4

Modeling flow and transport in brain extracellular space. (a) Jin et al. (2016) studied cerebrospinal fluid flow from periarterial to perivenous spaces on a hexagonal lattice estimating vessel locations in primate brain tissue and modeled the extracellular space with a geometric reconstruction that recapitulated the structure of tissue imaged by Kinney et al. (2013). Panel adapted from Jin et al. (2016) (CC BY-NC-SA 4.0). (b) Holter et al. (2017) simulated flow and transport in domains created by segmenting the 3D images of Kinney et al. (2013). Panel adapted from Holter et al. (2017) (CC BY 4.0). (c) Penetrating arterioles (*red*) and ascending venules (*blue*) in cortex extend roughly perpendicular to the brain surface, allowing for 2D modeling. Data from Pablo Blinder. (d) Taking arterioles and venules to be line sources and line sinks, respectively, and normalizing by the tissue permeability, Schreder et al. (2022) modeled flow and hydraulic resistance in both primate (not shown) and mouse brain tissue. Curves show streamlines. Panel adapted from Schreder et al. (2022); copyright 2022 the authors.

of the human fourth ventricle repeatedly followed modulations of neuronal activity during sleep. Measuring pressure is even more difficult than measuring flow, but pressure has important clinical implications. Accordingly, Sincomb et al. (2020) developed a model that can be used to estimate pressure from velocity in the aqueduct.

Flow in ventricles may also be driven by collective motion of the cilia that line ventricular walls. Siyahhan et al. (2014) performed simulations including both cardiac-driven wall motion and pumping by cilia, finding that wall motion was the primary driver of flow far from walls, but cilia were the primary driver of near-wall flow, and that cilia motion could impose a stronger directional flow than that driven by wall motion, which caused strong pulsations but little net motion.

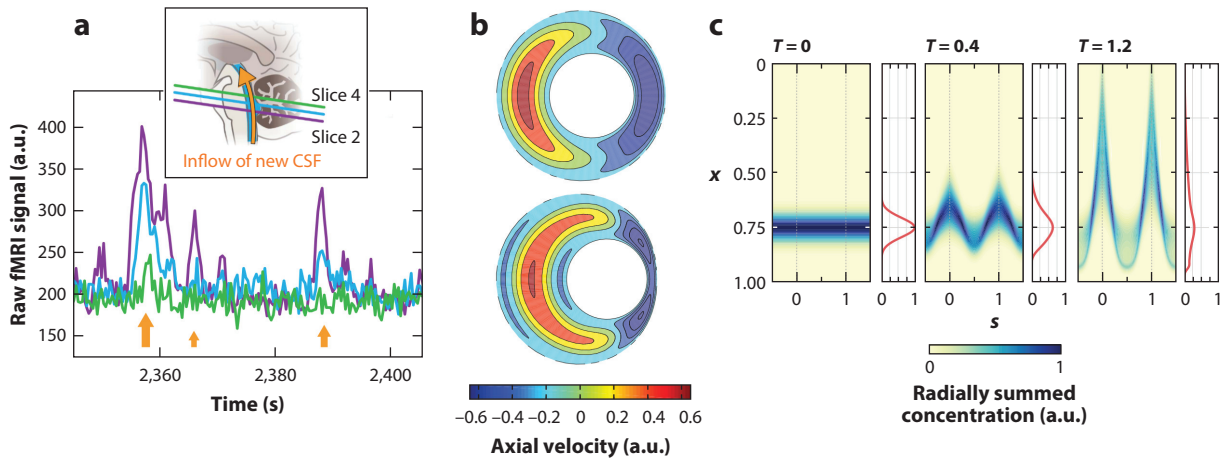


Figure 5

Cerebrospinal fluid (CSF) flow outside the brain. (a) Using functional magnetic resonance imaging (fMRI) in humans, Fultz et al. (2019) pulsed the magnetic field to excite water molecules in the field of view, and then measured as unexcited molecules were swept into the field of view by the flow of CSF. The raw signal grew earliest and most strongly in slices at the edge of the field of view, placed just below the fourth ventricle, indicating bulk fluid flow there. (b) Sánchez et al. (2018) developed an asymptotic fluid mechanical model for flow in the spinal subarachnoid space, driven by pressure fluctuations at its junction with the skull. The model predicts an axial streaming flow at second order, which varies depending on the eccentricity of the subarachnoid space, as shown here in cross section. (c) Lawrence et al. (2019) used the flow model of Sánchez et al. (2018) to simulate solute transport in the spinal subarachnoid space, with application to drug delivery. Here x is the axial coordinate, s is the azimuthal coordinate, T is time, and red curves show the concentration after summing over radius and azimuth. An initial bolus of solute is dispersed by the pulsing and streaming flow. Panels adapted with permission from (a) Fultz et al. (2019), copyright 2019 the authors; (b) Sánchez et al. (2018), copyright 2018 Cambridge University Press; and (c) Lawrence et al. (2019), copyright 2019 Cambridge University Press.

Faubel et al. (2016) studied tissue from rat and pig brains *in vitro*, quantifying both cilia motion and the resulting fluid flow in detail, concluding that cilia could drive complex flow patterns that might segregate solutes to certain regions of the ventricles, which vary between sleep and wakefulness.

CSF exiting and reentering the skull primarily communicates with the spinal canal, which, unlike the skull, can dilate and constrict to accommodate varying fluid volumes. The spinal subarachnoid space tapers to a close at its end, and like the much smaller penetrating PVSs, is annular. Flow there has implications for epidural drug delivery and for disorders including syringomyelia and Chiari malformation. Sánchez et al. (2018) idealized the canal as a linearly compliant, cylindrical, eccentric annulus that is subject to an oscillating pressure at its connection to the skull and closed on the other end. Thanks to the eccentricity, the model produced steady bulk flow in addition to the expected oscillations. Lawrence et al. (2019) used the same mathematical model to simulate drug transport in the spinal canal, finding much faster transport due to steady streaming than to Taylor dispersion for drugs of realistic diffusivity. Coenen et al. (2019) combined the mathematical model with MRI measurements of CSF velocity in the spinal canals of human subjects, allowing for patient-specific predictions of drug transport and revealing that recirculation regions play a key role but vary from patient to patient. Salerno et al. (2020) used simulations to find that trabeculae (small fibers spanning the spinal canal) significantly increase dispersion, consistent with prior predictions (Stockman 2007, Heidari Pahlavian et al. 2014). Vinje et al. (2018) investigated syringomyelia, combining MRI flow measurements with 2D simulations and finding that flows varied with heart rate, inlet velocities, and blockage diameter.

CSF flow outside the brain may, like flow within the brain, be significantly different during sleep than during wakefulness. Ma et al. (2019) imaged tracer motion in anesthetized mice, finding tracer primarily passing out of the skull along the spinal canal and lymph vessels, with little tracer entering the brain. From those results, the authors argued that fluid transport to brain tissue may be negligible. However, the isoflurane anesthesia they used may produce a flow state more like wakefulness than sleep (Hablitz et al. 2019). One hypothesis is that during wakefulness, when brain ECS shrinks (Xie et al. 2013) and its hydraulic resistance increases accordingly, fluid is shunted to spaces outside the brain, amplifying the flow there. That idea is supported by the facts that cardiac pulsation and functional hyperemia produce greater motion of artery walls during wakefulness than during sleep (Turner et al. 2020), and that simulations predict that cardiac and respiratory pressure gradients vary little from sleep to wakefulness (Vinje et al. 2019). Cardiac and respiratory frequencies also vary significantly from wakefulness to sleep. We hope that future studies will explore sleep–wake variation of CSF flow outside the brain.

7. SOLUTE TRANSPORT

Solute transport in the brain is accomplished by a combination of advection and diffusion: This combination is usually called dispersion by fluid dynamicists, but it has sometimes been called convection in the neuroscience literature (this term is also used as a synonym for advection, but we avoid using it here because of this ambiguity).

The basic equation governing the concentration C of a solute is the advection–diffusion equation

$$\frac{\partial C}{\partial t} + \mathbf{u} \cdot \nabla C = D \nabla^2 C + f, \quad 5.$$

where \mathbf{u} is the Eulerian velocity field, D is the diffusion coefficient, and f is the source term (the rate of generation of the solute per unit volume per unit time). CSF and ISF carry solutes at concentrations too low to alter flow; the viscosity and density remain essentially identical to that of water (Bloomfield et al. 1998). Thus, the velocity field \mathbf{u} can be considered as a known input to Equation 5. Although brain tissue is not homogeneous, if we consider length scales significantly larger than gap widths in the ECS, it is reasonably accurate to treat the tissue as a homogeneous, porous medium. In that case, the free diffusivity D must be replaced with an effective diffusivity $D^* = D/\lambda^2$, where λ is the tortuosity (Nicholson 2001). The tortuosity is the ratio of the average distance traveled by particles moving between two points and the straight-line distance between those two points (hence, $\lambda \geq 1$). In practice, the tortuosity is usually determined secondarily from tracer experiments that measure the effective diffusion coefficient D^* (Syková & Nicholson 2008, Nicholson & Hrabětová 2017). These experiments generally assume that there is no flow of ISF: The results are subject to reinterpretation if there is indeed a significant flow (see, for example, Ray et al. 2019). Tortuosity can also be predicted theoretically by means of structural models of the porous medium (Nicholson 2001). Tortuosity of more open spaces, such as surface PVSs, can be determined by means of particle-tracking (Min Rivas et al. 2020).

Although there is now abundant evidence for flow of CSF in the brain, and some evidence for flow of ISF, it is instructive to examine the hypothetical case in which there is no such flow anywhere in the interior of the brain, so that solute transport there is by diffusion alone. Consider a very simple model: steady-state diffusion in a homogeneous spherical brain (of radius a) in which the rate f of production of the solute is constant and uniform. Assume that the concentration is maintained at $C = 0$ at the surface of the brain, where solute is cleared quickly by a flow of CSF. The resulting concentration is then a function of the radial coordinate r only, and Equation 5

reduces to

$$\frac{1}{r^2} \frac{d}{dr} \left(r^2 \frac{dC}{dr} \right) = -\frac{f}{D^*}, \quad 6.$$

subject to the boundary condition $C = 0$ at $r = a$. The solution, easily obtained by direct integration, is

$$C(r) = \frac{f}{6D^*} (a^2 - r^2). \quad 7.$$

This concentration distribution $C(r)$ is parabolic, with maximum value $fa^2/6D^*$ at the center and minimum value at the surface. The brain is a large organ, so the appropriate radius a is large, and hence, the maximum concentration, which scales as a^2 , is inherently large. (Equating the volume of the sphere to the average volume of the human brain, $1,450 \text{ cm}^3$, gives a radius of about $a = 7 \text{ cm}$.) Note that the maximum concentration is proportional to the production rate f and inversely proportional to the effective diffusion coefficient D^* : Thus, for equal production rates, larger molecules, which have smaller effective diffusion coefficients, will have higher maximum concentrations and more nonuniform distributions. A healthy brain must regulate the concentrations of many different solutes at levels dictated by their biochemistry, not their size: If diffusion were the only clearance mechanism, this would not be possible.

Of course, the human brain is not spherical in shape, and its surface is corrugated (gyrencephalic), but in any more realistic model we would nonetheless expect highly nonuniform distributions of metabolic waste products, with maximum concentrations near the brain centroid and concentration gradients steepening (become more negative) toward the surface. Such distributions would be detrimental to brain function, and indeed there is no evidence that they exist: Accurate measurements of the distribution of a natural metabolite in the brain do not seem to have been carried out, but they would be very helpful in determining the relative contributions of advection and diffusion in the brain.

The relative importance of advection and diffusion is usually measured by a dimensionless number, the Péclet number Pe , which estimates the ratio of the advection and diffusion terms in Equation 5:

$$\frac{|\mathbf{u} \cdot \nabla C|}{|D \nabla^2 C|} \sim \frac{U(C_0/L)}{D(C_0/L^2)} \sim \frac{UL}{D} \equiv Pe, \quad 8.$$

where U is a velocity scale, C_0 is a typical value of the concentration, and L is a length scale for spatial variations in the concentration. In parts of the brain that are treated as porous, the free diffusivity D is replaced by the effective diffusivity D^* . For the flows in the periarterial spaces in the mouse brain (Mestre et al. 2018b), the Péclet number is large: $Pe \sim 1,000$ for the microspheres used in the experiments and $10 \leq Pe \leq 100$ for other relevant solutes. In these perivascular flows advection dominates diffusion. However, we do not expect this to be the case throughout the entire glymphatic system: The flow branches into many smaller PVSs along arterioles, precapillaries, venules, and veins and is much slower in these channels. Within the brain parenchyma, the flow of ISF is even slower, and Péclet numbers of order unity or less are to be expected.

The combined effects of advection and diffusion in a viscous flow along a narrow pipe produce Taylor dispersion (Taylor 1953, Aris 1956), in which the shear spreads solute in the streamwise direction while diffusion rapidly smooths out the concentration in the cross-stream direction, resulting in a large effective diffusion coefficient in the streamwise direction. Taylor dispersion will certainly occur in the flow of CSF along PVSs, although waste solutes will likely be entering a PVS rather uniformly along its length, so dispersion in the axial direction is not a major factor.

Due to uncertainties about the presence of a mean (bulk) flow, some have claimed that Taylor dispersion due to a purely oscillatory (zero-mean) flow in PVSs (driven by arterial pulsations) will provide effective clearance (Asgari et al. 2016, Faghiih & Sharp 2018, Sharp et al. 2019). However, Thomas (2019) argued, on qualitative grounds, that a purely oscillatory flow will produce only a slight increase in streamwise dispersion and no significant increase in clearance. Subsequent numerical simulations of dispersion in steady, oscillatory, and pulsatile flows in a model PVS (a concentric circular annular tube) confirmed that a purely oscillatory flow enhances axial dispersion only weakly, whereas a steady flow component, even if slow, clears waste much more effectively (Troyetsky et al. 2021).

8. GLOBAL MODELS

There have been a few attempts to model substantial portions of the CSF flow system in the brain. One such approach is to construct a hydraulic network model, based on the hydraulic Ohm's law (Equation 1). These models employ a branching network of 1D flow channels with different hydraulic resistances, representing different PVSs and other pathways in the system. Asgari et al. (2015) used a hydraulic network model to examine the possibility that some CSF passes through parallel pathways formed by astrocytes in going from arterial to venous PVSs. They showed that the inhibition of these pathways, caused by the deletion of the *AQP4* gene, reduces the volumetric flow between arterial and venous PVSs. Faghiih & Sharp (2018) presented a hydraulic network model of both the flow in PVSs and the proposed reverse flow in basement membranes (see Section 4.1): They found the flow to be too slow to be significant for reasonable values of the driving pressure gradient. Tithof et al. (2022) modeled the flow of CSF and ISF using a hydraulic network that accounts for PVSs surrounding surface arteries, penetrating arterioles, precapillaries, gaps between astrocyte endfeet, and the ECS, based on detailed experimental measurements of the vascular connectivity (Blinder et al. 2010, 2013). They explored the ranges of uncertainties of various input parameters, such as the size of precapillary PVSs and the permeability of brain tissue, and concluded that a combination of low-resistance PVSs and high-resistance tissue best explains experimental observations and that wake-sleep variations are best explained when tissue hydraulic resistance accounts for most of the network resistance. Boster et al. (2022) performed sensitivity analysis on the same model and found that uncertainty in the permeability of penetrating PVSs affects model predictions more than any other parameter, urging that it be measured precisely in experiments. Mestre et al. (2020a) developed a network model for CSF flow along PVSs during stroke. In their model, a spreading depolarization wave, induced by lack of blood flow, causes local constriction of surface and penetrating arteries, effectively enlarging PVSs and sucking CSF into them. This network model differs from others in that temporal variations are explicitly incorporated but hydraulic resistance does not play a key role.

All of these network models suffer from the large uncertainties in the values of several key parameters. The hydraulic resistance of an open space through which CSF flows in a laminar matter scales as L^{-4} (where L is the characteristic lateral size) so that minor uncertainty about the geometry of surface PVSs has a major effect. Penetrating PVSs may be open spaces subject to the same sort of uncertainty or may be filled with a porous medium, in which case the permeability is entirely unknown. Beyond PVSs, published estimates of the permeability of brain tissue vary over more than two orders of magnitude, and published estimates of the gap width between astrocyte endfeet vary over more than three orders of magnitude (Tithof et al. 2022). Although these quantities are difficult to measure, improving their accuracy is essential for advancing the field.

One way to avoid the challenge of describing the microscale anatomy is to model the CSF flow system in terms of connected control volumes, typically called compartment models or pharmacokinetic models. Once the volumes of interest are demarcated, conservation laws for each (e.g., fluid mass, solute mass, momentum) can be expressed as a combination of creation/annihilation in place and inflow/outflow from other volumes, perhaps connected via hydraulic resistances. Vinje et al. (2020) used a compartment model to explore whether pressure increases caused by tracer injection might reroute CSF flow and found strong effects, but that conclusion comes as no surprise because compliance was presumed to depend on pressure. Linninger et al. (2009) produced a pioneering compartment model linking CSF flow to blood flow. Compartment models can be especially powerful when combined with in vivo measurements. Elbert et al. (2022) combined a compartment model with measurements of radioactively tagged amyloid beta in humans, finding that amyloid removal seems to be achieved through a combination of CSF flow, enzymatic protein breakdown, and transport across the BBB, with CSF flow weakening the least with age.

SUMMARY POINTS

1. Flows of cerebrospinal fluid (CSF) and interstitial fluid (ISF) in the central nervous system constitute a fluid transport system, often called the glymphatic system, that provides nutrients to the brain and sweeps away metabolic wastes.
2. Glymphatic flow and transport in brain tissue occur almost exclusively during sleep, when the extracellular space (ECS) there is roughly 60% larger than during wakefulness. Flow and transport in the spinal canal, brain ventricles, and brain subarachnoid space proceed (and may be enhanced) during wakefulness.
3. CSF flow is tightly coupled to blood flow because the rigid skull constrains both, and because CSF often follows perivascular spaces (PVSs) surrounding blood vessels. On average, CSF in surface periarterial spaces flows in the same direction as blood and pulses in synchrony with the heart (although the respiration frequency is evident in CSF flow elsewhere).
4. At least some CSF from surface PVSs enters the brain along PVSs surrounding penetrating arterioles.
5. Solutes are transported through the brain ECS thanks to a combination of advection and diffusion, with Péclet number $Pe \sim 1$.
6. Flow in the spinal canal is driven primarily by flow of CSF into and out of the rigid skull, modulated by both the cardiac and respiratory cycles. A steady streaming arises and can be used for drug delivery, subverting the blood–brain barrier.

FUTURE ISSUES

1. What are the driving mechanisms for the flow of CSF along PVSs?
2. What are the relative contributions of advection and diffusion in the ISF in the ECSs?
3. What fluid dynamical mechanisms regulate the wake-to-sleep increase in glymphatic flow and waste clearance?

4. What are the characteristics and biological roles of flows in ventricles and subarachnoid spaces?
5. Can glymphatic transport be modulated to improve delivery of therapeutic drugs to the central nervous system, reduce dangerous swelling during stroke and cardiac arrest, and prevent waste accumulation associated with aging and neurodegeneration?

DISCLOSURE STATEMENT

The authors are not aware of any biases that might be perceived as affecting the objectivity of this review.

ACKNOWLEDGMENTS

We thank Maiken Nedergaard for introducing us to research on CSF flow, and we thank her, Humberto Mestre, Jessica Shang, Jeff Tithof, Aditya Raghunandan, and Kimberly Boster for many helpful discussions. We thank Dan Xue for expert illustration. Preparation of this review was supported by the NIH (National Institutes of Health)/NIA (National Institute of Aging) (grant RF1AG057575) and by the US Army Research Office (grant MURI W911NF1910280).

LITERATURE CITED

- Abbott NJ. 2004. Evidence for bulk flow of brain interstitial fluid: significance for physiology and pathology. *Neurochem. Int.* 45(4):545–52
- Ahn JH, Cho H, Kim JH, Kim SH, Ham JS, et al. 2019. Meningeal lymphatic vessels at the skull base drain cerebrospinal fluid. *Nature* 572:62–66
- Albargothy NJ, Johnston DA, MacGregor-Sharp M, Weller RO, Verma A, et al. 2018. Convective in-flux/glymphatic system: Tracers injected into the CSF enter and leave the brain along separate periarterial basement membrane pathways. *Acta Neuropathol.* 136(1):139–52
- Aris R. 1956. On the dispersion of a solute in a fluid flowing through a tube. *Proc. R. Soc. A* 235(1200):67–77
- Asgari M, de Zélicourt D, Kurtcuoglu V. 2015. How astrocyte networks may contribute to cerebral metabolite clearance. *Sci. Rep.* 5:15024
- Asgari M, de Zélicourt D, Kurtcuoglu V. 2016. Glymphatic solute transport does not require bulk flow. *Sci. Rep.* 6:38635
- Aspelund A, Antila S, Proulx ST, Karlsen TV, Karaman S, et al. 2015. A dural lymphatic vascular system that drains brain interstitial fluid and macromolecules. *J. Exp. Med.* 212(7):991–99
- Avrahami I, Gharib M. 2008. Computational studies of resonance wave pumping in compliant tubes. *J. Fluid Mech.* 608:205–22
- Basser PJ. 1992. Interstitial pressure, volume, and flow during infusion into brain tissue. *Microvasc. Res.* 44(2):143–65
- Bèchet NB, Shanbhag NC, Lundgaard I. 2021. Glymphatic pathways in the gyrencephalic brain. *J. Cerebr. Blood Flow Metab.* 41(9):2264–79
- Bedussi B, Almasian M, de Vos J, VanBavel E, Bakker ENTP. 2018. Paravascular spaces at the brain surface: low resistance pathways for cerebrospinal fluid flow. *J. Cerebr. Blood Flow Metab.* 38(4):719–26
- Benveniste H, Lee H, Ozturk B, Chen X, Koundal S, et al. 2020. Glymphatic cerebrospinal fluid and solute transport quantified by MRI and PET imaging. *Neuroscience* 474:63–79
- Benveniste H, Liu X, Koundal S, Sanggaard S, Lee H, Wardlaw J. 2019. The glymphatic system and waste clearance with brain aging: a review. *Gerontology* 65(2):106–19
- Bilston LE, Fletcher DF, Brodbelt AR, Stoodley MA. 2003. Arterial pulsation-driven cerebrospinal fluid flow in the perivascular space: a computational model. *Comput. Methods Biomech.* 6(4):235–41

- Blinder P, Shih AY, Rafie C, Kleinfeld D. 2010. Topological basis for the robust distribution of blood to rodent neocortex. *PNAS* 107(28):12670–75
- Blinder P, Tsai PS, Kaufhold JP, Knutsen PM, Suhl H, Kleinfeld D. 2013. The cortical angiome: an interconnected vascular network with noncolumnar patterns of blood flow. *Nat. Neurosci.* 16(7):889
- Bloomfield IG, Johnston IH, Bilston LE. 1998. Effects of proteins, blood cells and glucose on the viscosity of cerebrospinal fluid. *Pediatr. Neurosurg.* 28(5):246–51
- Bohr T, Hjorth PG, Holst SC, Hrabětová S, Kiviniemi V, et al. 2022. The glymphatic system: current understanding and modeling. *iScience* 25(9):104987
- Boster KAS, Tithof J, Cook DD, Thomas JH, Kelley DH. 2022. Sensitivity analysis on a network model of glymphatic flow. *J. R. Soc. Interface* 19:20220257
- Carare RO, Bernardes-Silva M, Newman TA, Page AM, Nicoll JA, et al. 2008. Solutes, but not cells, drain from the brain parenchyma along basement membranes of capillaries and arteries: significance for cerebral amyloid angiopathy and neuroimmunology. *Neuropathol. Appl. Neurobiol.* 34(2):131–44
- Carr JB, Thomas JH, Liu J, Shang JK. 2021. Peristaltic pumping in thin non-axisymmetric annular tubes. *J. Fluid Mech.* 917:A10
- Chen X, Liu X, Koundal S, Elkin R, Zhu X, et al. 2022. Cerebral amyloid angiopathy is associated with glymphatic transport reduction and time-delayed solute drainage along the neck arteries. *Nat. Aging* 2:214–223
- Coenen W, Gutiérrez-Montes C, Sincomb S, Criado-Hidalgo E, Wei K, et al. 2019. Subject-specific studies of CSF bulk flow patterns in the spinal canal: implications for the dispersion of solute particles in intrathecal drug delivery. *Am. J. Neuroradiol.* 40(7):1242–49
- Coenen W, Zhang X, Sánchez AL. 2021. Lubrication analysis of peristaltic motion in non-axisymmetric annular tubes. *J. Fluid Mech.* 921:R2
- Colbourn R, Hrabec J, Nicholson C, Perkins M, Goodman JH, Hrabetova S. 2021. Rapid volume pulsation of the extracellular space coincides with epileptiform activity in mice and depends on the NBCe1 transporter. *J. Physiol.* 599(12):3195–220
- Coloma M, Schaffer JD, Carare RO, Chiarot PR, Huang P. 2016. Pulsations with reflected boundary waves: a hydrodynamic reverse transport mechanism for perivascular drainage in the brain. *J. Math. Biol.* 73(2):469–90
- Coloma M, Schaffer JD, Huang P, Chiarot PR. 2019. Boundary waves in a microfluidic device as a model for intramural periarterial drainage. *Biomicrofluidics* 13(2):024103–12
- Croci M, Vinje V, Rognes ME. 2019. Uncertainty quantification of parenchymal tracer distribution using random diffusion and convective velocity fields. *Fluids Barriers CNS* 16:32
- Cserr HF, Cooper D, Milhorat T. 1977. Flow of cerebral interstitial fluid as indicated by the removal of extracellular markers from rat caudate nucleus. *Exp. Eye Res.* 25:461–73
- Cserr HF, Cooper DN, Suri PK, Patlak CS. 1981. Efflux of radiolabeled polyethylene glycols and albumin from rat brain. *Am. J. Physiol. Renal Physiol.* 240(4):F319–28
- Daversin-Catty C, Gjerde IG, Rognes ME. 2021. Geometrically reduced modelling of pulsatile flow in perivascular networks. *Front. Phys.* 10:882260
- de Guevara AL, Shang JK, Nedergaard M, Kelley DH. 2022. Perivascular pumping in the mouse brain: improved boundary conditions reconcile theory, simulation, and experiment. *J. Theor. Biol.* 542:111103
- Du T, Mestre H, Kress BT, Liu G, Sweeney AM, et al. 2021. Cerebrospinal fluid is a significant fluid source for anoxic cerebral oedema. *Brain* 145(2):787–97
- Eide PK, Holm S, Sorteberg W. 2012. Simultaneous monitoring of static and dynamic intracranial pressure parameters from two separate sensors in patients with cerebral bleeds: comparison of findings. *BioMed. Eng. OnLine* 11:66
- Eide PK, Vinje V, Pripp AH, Mardal KA, Ringstad G. 2021. Sleep deprivation impairs molecular clearance from the human brain. *Brain* 144(3):863–74
- Elbert DL, Patterson BW, Lucey BP, Benzinger TLS, Bateman RJ. 2022. Importance of CSF-based A β clearance with age in humans increases with declining efficacy of blood-brain barrier/proteolytic pathways. *Commun. Biol.* 5:98
- Faghii MM, Sharp MK. 2018. Is bulk flow plausible in perivascular, paravascular and paravenous channels? *Fluids Barriers CNS* 15:17

- Faghih MM, Sharp MK. 2021. Mechanisms of tracer transport in cerebral perivascular spaces. *J. Biomech.* 118:110278
- Faubel R, Westendorf C, Bodenschatz E, Eichele G. 2016. Cilia-based flow network in the brain ventricles. *Science* 353(6295):176–78
- Freund JB. 2014. Numerical simulation of flowing blood cells. *Annu. Rev. Fluid Mech.* 46:67–95
- Fultz NE, Bonmassar G, Setsompop K, Stickgold RA, Rosen BR, et al. 2019. Coupled electrophysiological, hemodynamic, and cerebrospinal fluid oscillations in human sleep. *Science* 366:628–31
- Gjerde I, Rognes M. 2021. A mixed framework for topological model reduction of coupled PDEs. In *International Conference on Computational Methods for Coupled Problems in Science and Engineering (COUPLED PROBLEMS 2021)*, ed. E Oñate, M Papadarakakis, B Schrefler. Barcelona: Int. Cent. Numer. Methods Eng. https://www.scipedia.com/public/Gjerde_Rognes_2021a
- Godin AG, Varela JA, Gao Z, Danne N, Dupuis JP, et al. 2017. Single-nanotube tracking reveals the nanoscale organization of the extracellular space in the live brain. *Nat. Nanotechnol.* 12(3):238–43
- Hablitz LM, Nedergaard M. 2021a. The glymphatic system. *Curr. Biol.* 31(20):R1371–75
- Hablitz LM, Nedergaard M. 2021b. The glymphatic system: a novel component of fundamental neurobiology. *J. Neurosci.* 41(37):7698–711
- Hablitz LM, Pla V, Giannetto M, Vnitsky HS, Staeger FF, et al. 2020. Circadian control of brain glymphatic and lymphatic fluid flow. *Nat. Commun.* 11:4411
- Hablitz LM, Vnitsky HS, Sun Q, Staeger FF, Sigurdsson B, et al. 2019. Increased glymphatic influx is correlated with high EEG delta power and low heart rate in mice under anesthesia. *Sci. Adv.* 5(2):eaav5447
- Hadaczek P, Yamashita Y, Mirek H, Tamas L, Bohn MC, et al. 2006. The “perivascular pump” driven by arterial pulsation is a powerful mechanism for the distribution of therapeutic molecules within the brain. *Mol. Ther.* 14(1):69–78
- Halnes G, Østby I, Pettersen KH, Omhold SW, Einevoll GT. 2013. Electrodifusive model for astrocytic and neuronal ion concentration dynamics. *PLoS Comput. Biol.* 9:e1003386
- Hannocks MJ, Pizzo ME, Huppert J, Deshpande T, Abbott NJ, et al. 2018. Molecular characterization of perivascular drainage pathways in the murine brain. *J. Cereb. Blood Flow Metab.* 38(4):669–86
- Heidari Pahlavian S, Yiallourou T, Tubbs RS, Bunck AC, Loth F, et al. 2014. The impact of spinal cord nerve roots and denticulate ligaments on cerebrospinal fluid dynamics in the cervical spine. *PLOS ONE* 9(4):e91888
- Hickerson AI, Gharib M. 2006. On the resonance of a pliant tube as a mechanism for valveless pumping. *J. Fluid Mech.* 555:141–48
- Hladky SB, Barrand MA. 2014. Mechanisms of fluid movement into, through, and out of the brain: evolution of the evidence. *Fluids Barriers CNS* 11:26
- Hladky SB, Barrand MA. 2018. Elimination of substances from the brain parenchyma: efflux via perivascular pathways and via the blood–brain barrier. *Fluids Barriers CNS* 15:30
- Hladky SB, Barrand MA. 2022. The glymphatic hypothesis: the theory and the evidence. *Fluids Barriers CNS* 19:9
- Holter KE, Kehlet B, Devor A, Sejnowski TJ, Dale AM, et al. 2017. Interstitial solute transport in 3D reconstructed neuropil occurs by diffusion rather than bulk flow. *PNAS* 114(37):9894–99
- Hrabe J, Hrabětova S. 2019. Time-resolved integrative optical imaging of diffusion during spreading depression. *Biophys. J.* 117(10):1783–94
- Ichimura T, Fraser PA, Cserr HF. 1991. Distribution of extracellular tracers in perivascular spaces of the rat brain. *Brain Res.* 545(1–2):103–13
- Iliff J, Wang M, Liao Y, Plogg B, Peng W, et al. 2012. A paravascular pathway facilitates CSF flow through the brain parenchyma and the clearance of interstitial solutes, including amyloid β . *Sci. Transl. Med.* 4(147):147ra111
- Iliff J, Wang M, Zeppenfeld D, Venkataraman A, Plog B, et al. 2013. Cerebral arterial pulsation drives paravascular CSF–interstitial fluid exchange in the murine brain. *J. Neurosci.* 33(46):18190–99
- Jaffrin MY, Shapiro AH. 1971. Peristaltic pumping. *Annu. Rev. Fluid Mech.* 3:13–37
- Jessen N, Munk A, Lundgaard I, Nedergaard M. 2015. The glymphatic system: a beginner’s guide. *Neurochem. Res.* 40(12):2583–99

- Jin BJ, Smith AJ, Verkman AS. 2016. Spatial model of convective solute transport in extracellular space does not support a “glymphatic” mechanism. *J. Gen. Physiol.* 148(6):489–501
- Johnston M, Papaiconomou C. 2002. Cerebrospinal fluid transport: a lymphatic perspective. *Physiology* 17(6):227–30
- Kedarasetti R, Drew PJ, Costanzo F. 2021. Arterial vasodilation drives convective fluid flow in the brain: a poroelastic model. *Fluids Barriers CNS* 19:34
- Kedarasetti RT, Drew PJ, Costanzo F. 2020a. Arterial pulsations drive oscillatory flow of CSF but not directional pumping. *Sci. Rep.* 10:10102
- Kedarasetti RT, Turner KL, Echagarruga C, Gluckman BJ, Drew PJ, Costanzo F. 2020b. Functional hyperemia drives fluid exchange in the paravascular space. *Fluids Barriers CNS* 17:52
- Kelley DH. 2021. Brain cerebrospinal fluid flow. *Phys. Rev. Fluids* 6:070501
- Kinney JP, Spacek J, Bartol TM, Bajaj CL, Harris KM, Sejnowski TJ. 2013. Extracellular sheets and tunnels modulate glutamate diffusion in hippocampal neuropil. *J. Comp. Neurol.* 521(2):448–64
- Koundal S, Elkin R, Nadeem S, Xue Y, Constantinou S, et al. 2020. Optimal mass transport with Lagrangian workflow reveals advective and diffusion driven solute transport in the glymphatic system. *Sci. Rep.* 10:1990
- Kress B, Iliff J, Xia M, Wang M, Wei H, et al. 2014. Impairment of paravascular clearance pathways in the aging brain. *Ann. Neurol.* 76(6):845–61
- Ku DN. 1997. Blood flow in arteries. *Annu. Rev. Fluid Mech.* 29:399–434
- Lam MA, Hemley SJ, Najafi E, Vella NGF, Bilston LE, Stoodley MA. 2017. The ultrastructure of spinal cord perivascular spaces: implications for the circulation of cerebrospinal fluid. *Sci. Rep.* 7:12924
- Lawrence JJ, Coenen W, Sánchez AL, Pawiak G, Martínez-Bazán C, et al. 2019. On the dispersion of a drug delivered intrathecally in the spinal canal. *J. Fluid Mech.* 861:679–720
- Lilius TO, Blomqvist K, Hauglund NL, Liu G, Ståger FF, et al. 2019. Dexmedetomidine enhances glymphatic brain delivery of intrathecally administered drugs. *J. Control. Release* 304:29–38
- Linninger AA, Somayaji MR, Erickson T, Guo X, Penn RD. 2008. Computational methods for predicting drug transport in anisotropic and heterogeneous brain tissue. *J. Biomech.* 41(10):2176–87
- Linninger AA, Tången K, Hsu CY, Frim D. 2016. Cerebrospinal fluid mechanics and its coupling to cerebrovascular dynamics. *Annu. Rev. Fluid Mech.* 48:219–57
- Linninger AA, Xenos M, Sweetman B, Ponshe S, Guo X, Penn R. 2009. A mathematical model of blood, cerebrospinal fluid and brain dynamics. *J. Math. Biol.* 59(6):729–59
- Louveau A, Smirnov I, Keyes TJ, Eccles JD, Rouhani SJ, et al. 2015. Structural and functional features of central nervous system lymphatic vessels. *Nature* 523(7560):337–41
- Ma Q, Ineichen BV, Detmar M, Proulx ST. 2017. Outflow of cerebrospinal fluid is predominantly through lymphatic vessels and is reduced in aged mice. *Nat. Commun.* 8:1434
- Ma Q, Ries M, Decker Y, Müller A, Riner C, et al. 2019. Rapid lymphatic efflux limits cerebrospinal fluid flow to the brain. *Acta Neuropathol.* 137:151–65
- Magdoom KN, Brown A, Rey J, Mareci TH, King MA, Sarntinoranont M. 2019. MRI of whole rat brain perivascular network reveals role for ventricles in brain waste clearance. *Sci. Rep.* 9:11480
- Mesquita S, Louveau A, Vaccari A, Smirnov I, Cornelison RC, et al. 2018. Functional aspects of meningeal lymphatics in ageing and Alzheimer’s disease. *Nature* 560:185–91
- Mestre H, Du T, Sweeney AM, Liu G, Samson AJ, et al. 2020a. Cerebrospinal fluid influx drives acute ischemic tissue swelling. *Science* 367(6483):eaax7171
- Mestre H, Hablitz LM, Xavier ALR, Feng W, Zou W, et al. 2018a. Aquaporin-4-dependent glymphatic solute transport in the rodent brain. *eLife* 7:e40070
- Mestre H, Mori Y, Nedergaard M. 2020b. The brain’s glymphatic system: current controversies. *Trends Neurosci.* 43(7):458–66
- Mestre H, Tithof J, Du T, Song W, Peng W, et al. 2018b. Flow of cerebrospinal fluid is driven by arterial pulsations and is reduced in hypertension. *Nat. Commun.* 9:4878
- Min Rivas F, Liu J, Martell BC, Du T, Mestre H, et al. 2020. Surface periarterial spaces in the mouse brain are open, not porous. *J. R. Soc. Interface* 17:20200593
- Moore JE, Bertram CD. 2018. Lymphatic system flows. *Annu. Rev. Fluid Mech.* 50:459–82

- Nägerl UV, Willig KI, Hein B, Hell SW, Bonhoeffer T. 2008. Live-cell imaging of dendritic spines by steric microscopy. *PNAS* 105(48):18982–87
- Nedergaard M. 2013. Garbage truck of the brain. *Science* 340(6140):1529–30
- Nedergaard M, Goldman SA. 2020. Glymphatic failure as a final common pathway to dementia. *Science* 370(6512):50–56
- Nicholson C. 2001. Diffusion and related transport mechanisms in brain tissue. *Rep. Prog. Phys.* 64:815–84
- Nicholson C, Hrabětová S. 2017. Brain extracellular space: the final frontier of neuroscience. *Biophys. J.* 113(10):2133–42
- Nicholson C, Phillips J. 1981. Ion diffusion modified by tortuosity and volume fraction in the extracellular microenvironment of the rat cerebellum. *J. Physiol.* 321:225–57
- Nicholson C, Tao L. 1993. Hindered diffusion of high molecular weight compounds in brain extracellular microenvironment measured with integrative optical imaging. *Biophys. J.* 65(6):2277–90
- Paviolo C, Soria FN, Ferreira JS, Lee A, Groc L, et al. 2020. Nanoscale exploration of the extracellular space in the live brain by combining single carbon nanotube tracking and super-resolution imaging analysis. *Methods* 174:91–99
- Peng SL, Dumas JA, Park DC, Liu P, Filbey FM, et al. 2014. Age-related increase of resting metabolic rate in the human brain. *NeuroImage* 98:176–83
- Petitclerc L, Hirschler L, Wells JA, Thomas DL, van Walderveen MA, et al. 2021. Ultra-long-TE arterial spin labeling reveals rapid and brain-wide blood-to-CSF water transport in humans. *NeuroImage* 245:118755
- Pizzo ME, Wolak DJ, Kumar NN, Brunette E, Brunnquell CL, et al. 2018. Intrathecal antibody distribution in the rat brain: surface diffusion, perivascular transport and osmotic enhancement of delivery. *J. Physiol.* 596(3):445–75
- Plog BA, Mestre H, Olveda GE, Sweeney AM, Kenney HM, et al. 2018. Transcranial optical imaging reveals a pathway for optimizing the delivery of immunotherapeutics to the brain. *JCI Insight* 3(20):e120922
- Plog BA, Nedergaard M. 2018. The glymphatic system in central nervous system health and disease: past, present, and future. *Ann. Rev. Pathol.* 13:379–94
- Raghubandan A, Ladron-de Guevera A, Tithof J, Mestre H, Du T, et al. 2021. Bulk flow of cerebrospinal fluid observed in periarterial spaces is not an artifact of injection. *eLife* 10:e65958
- Rasmussen MK, Mestre H, Nedergaard M. 2018. The glymphatic pathway in neurological disorders. *Lancet Neurol.* 17(11):1016–24
- Rasmussen MK, Mestre H, Nedergaard M. 2022. Fluid transport in the brain. *Physiol. Rev.* 102(2):1025–151
- Ratner V, Gao Y, Lee H, Elkin R, Nedergaard M, et al. 2017. Cerebrospinal and interstitial fluid transport via the glymphatic pathway modeled by optimal mass transport. *NeuroImage* 152:530–37
- Ray LA, Heys JJ. 2019. Fluid flow and mass transport in brain tissue. *Fluids* 4(4):196
- Ray LA, Iliff JJ, Heys JJ. 2019. Analysis of convective and diffusive transport in the brain interstitium. *Fluids Barriers CNS* 16:6
- Ray LA, Pike M, Simon M, Iliff JJ, Heys JJ. 2021. Quantitative analysis of macroscopic solute transport in the murine brain. *Fluids Barriers CNS* 18:55
- Rennels ML, Gregory TF, Blaumanis OR, Fujimoto K, Grady PA. 1985. Evidence for a ‘paravascular’ fluid circulation in the mammalian central nervous system, provided by the rapid distribution of tracer protein throughout the brain from the subarachnoid space. *Brain Res.* 326(1):47–63
- Rey J, Sartinoranont M. 2018. Pulsatile flow drivers in brain parenchyma and perivascular spaces: a resistance network model study. *Fluids Barriers CNS* 15:20
- Ringstad G, Våtnes SAS, Eide PK. 2017. Glymphatic MRI in idiopathic normal pressure hydrocephalus. *Brain* 140(10):2691–705
- Romanò F, Suresh V, Galie PA, Grothberg JB. 2020. Peristaltic flow in the glymphatic system. *Sci. Rep.* 10:21065
- Salerno L, Cardillo G, Camporeale C. 2020. Aris-Taylor dispersion in the subarachnoid space. *Phys. Rev. Fluids* 5(4):043102
- Sánchez AL, Martínez-Bazán C, Gutiérrez-Montes C, Criado-Hidalgo E, Pawlak G, et al. 2018. On the bulk motion of the cerebrospinal fluid in the spinal canal. *J. Fluid Mech.* 841:203–27
- Schain AJ, Melo-Carrillo A, Strassman AM, Burstein R. 2017. Cortical spreading depression closes paravascular space and impairs glymphatic flow: implications for migraine headache. *J. Neurosci.* 37(11):2904–15

- Schley D, Carare-Nnadi R, Please CP, Perry VH, Weller RO. 2006. Mechanisms to explain the reverse perivascular transport of solutes out of the brain. *J. Theor. Biol.* 238(4):962–74
- Schreder HE, Liu J, Kelley DH, Thomas JH, Boster KAS. 2022. Hydraulic resistance model for interstitial flow in the brain. *J. R. Soc. Interface* 19:20210812
- Secomb TW. 2017. Blood flow in the microcirculation. *Annu. Rev. Fluid Mech.* 49:443–61
- Sharp MK, Carare RO, Martin BA. 2019. Dispersion in porous media in oscillatory flow between flat plates: applications to intrathecal, periarterial and paraarterial solute transport in the central nervous system. *Fluids Barriers CNS* 16:13
- Sincomb S, Coenen W, Gutiérrez-Montes C, Martínez Bazán C, Haughton V, Sánchez AL. 2022. A one-dimensional model for the pulsating flow of cerebrospinal fluid in the spinal canal. *J. Fluid Mech.* 939:A26
- Sincomb S, Coenen W, Sánchez AL, Lasheras JC. 2020. A model for the oscillatory flow in the cerebral aqueduct. *J. Fluid Mech.* 899:R1
- Siyahhan B, Knobloch V, de Zélicourt D, Asgari M, Schmid Daners M, et al. 2014. Flow induced by ependymal cilia dominates near-wall cerebrospinal fluid dynamics in the lateral ventricles. *J. R. Soc. Interface* 11(94):20131189–10
- Smith AJ, Verkman AS. 2018. The “glymphatic” mechanism for solute clearance in Alzheimer’s disease: game changer or unproven speculation? *FASEB J.* 32(2):543–51
- Smith AJ, Yao X, Dix JA, Jin BJ, Verkman AS. 2017. Test of the ‘glymphatic’ hypothesis demonstrates diffusive and aquaporin-4-independent solute transport in rodent brain parenchyma. *eLife* 6:e27679
- Stanton EH, Persson NDA, Gomolka RS, Lilius T, Sigurosson B, et al. 2021. Mapping of CSF transport using high spatiotemporal resolution dynamic contrast-enhanced MRI in mice: effect of anesthesia. *Magnet. Resonan. Med.* 85(6):3326–42
- Stockman HW. 2007. Effect of anatomical fine structure on the dispersion of solutes in the spinal subarachnoid space. *J. Biomech. Eng.* 129:666–75
- Syková E, Nicholson C. 2008. Diffusion in brain extracellular space. *Physiol. Rev.* 88(4):1277–340
- Szentistványi I, Patlak CS, Ellis RA, Cserr HF. 1984. Drainage of interstitial fluid from different regions of rat brain. *Am. J. Physiol.* 246(6 Part 2):F835–44
- Tangen KM, Hsu Y, Zhu DC, Linninger AA. 2015. CNS wide simulation of flow resistance and drug transport due to spinal microanatomy. *J. Biomech.* 48(10):2144–54
- Taylor GI. 1953. Dispersion of soluble matter in solvent flowing slowly through a tube. *Proc. R. Soc. A* 219(1137):186–203
- Thomas JH. 2019. Fluid dynamics of cerebrospinal fluid flow in perivascular spaces. *J. R. Soc. Interface* 16:20190572
- Thomas JH. 2022. Changes in waste clearance in the brain from wake to sleep suggest a flow of interstitial fluid. *Fluids Barriers CNS* 19:30
- Tithof J, Boster KAS, Bork PAR, Nedergaard M, Thomas JH, Kelley DH. 2022. A network model of glymphatic flow under different experimentally-motivated parametric scenarios. *iScience* 25(5):104258
- Tithof J, Kelley DH, Mestre H, Nedergaard M, Thomas JH. 2019. Hydraulic resistance of periarterial spaces in the brain. *Fluids Barriers CNS* 16:19
- Tønnesen J, Inavalli VVG, Nägerl UV. 2018. Super-resolution imaging of the extracellular space in living brain tissue. *Cell* 172(5):1108–21.e15
- Troyetsky DE, Tithof J, Thomas JH, Kelley DH. 2021. Dispersion as a waste-clearance mechanism in flow through penetrating perivascular spaces in the brain. *Sci. Rep.* 11:4595
- Turner KL, Gheres KW, Proctor EA, Drew PJ. 2020. Neurovascular coupling and bilateral connectivity during NREM and REM sleep. *eLife* 9:e62071
- Valnes LM, Mitusch SK, Ringstad G, Eide PK, Funke SW, Mardal KA. 2020. Apparent diffusion coefficient estimates based on 24 hours tracer movement support glymphatic transport in human cerebral cortex. *Sci. Rep.* 10:9176
- van Veluw SJ, Hou SS, Calvo-Rodriguez M, Arbel-Ornath M, Snyder AC, et al. 2020. Vasomotion as a driving force for paravascular clearance in the awake mouse brain. *Neuron* 105(3):549–61
- Vardakis JC, Chou D, Guo L, Ventikos Y. 2020. Exploring neurodegenerative disorders using a novel integrated model of cerebral transport: initial results. *Proc. Inst. Mech. Eng. H* 234(11):1223–34

- Vinje V, Bakker ENTP, Rognes ME. 2021. Brain solute transport is more rapid in periarterial than perivenous spaces. *Sci. Rep.* 11:16085
- Vinje V, Brucker J, Rognes ME, Mardal KA, Haughton V. 2018. Fluid dynamics in syringomyelia cavities: effects of heart rate, CSF velocity, CSF velocity waveform and craniovertebral decompression. *Neuroradiol. J.* 31(5):482–89
- Vinje V, Eklund A, Mardal KA, Rognes ME, Støverud KH. 2020. Intracranial pressure elevation alters CSF clearance pathways. *Fluids Barriers CNS* 17:29
- Vinje V, Ringstad G, Lindstrøm EK, Valnes LM, Rognes ME, et al. 2019. Respiratory influence on cerebrospinal fluid flow—a computational study based on long-term intracranial pressure measurements. *Sci. Rep.* 9:9732
- Wang MX, Ray L, Tanaka KF, Iliff JJ, Heys J. 2021. Varying perivascular astroglial endfoot dimensions along the vascular tree maintain perivascular-interstitial flux through the cortical mantle. *Glia* 69:715–28
- Wang P, Olbricht WL. 2011. Fluid mechanics in the perivascular space. *J. Theor. Biol.* 274(1):52–57
- Wardlaw JM, Benveniste H, Nedergaard M, Zlokovic BV, Mestre H, et al. 2020. Perivascular spaces in the brain: anatomy, physiology and pathology. *Nat. Rev. Neurol.* 16(3):137–53
- White FM. 2006. *Viscous Fluid Flow*. New York: McGraw-Hill. 3rd ed.
- Xie L, Kang H, Xu Q, Chen MJ, Liao Y, et al. 2013. Sleep drives metabolite clearance from the adult brain. *Science* 342(6156):373–77
- Yildiz S, Thyagaraj S, Jin N, Zhong X, Heidari Pahlavian S, et al. 2017. Quantifying the influence of respiration and cardiac pulsations on cerebrospinal fluid dynamics using real-time phase-contrast MRI. *J. Magnet. Resonan. Imaging* 46(2):431–39
- Yokoyama N, Takeishi N, Wada S. 2021. Cerebrospinal fluid flow driven by arterial pulsations in axisymmetric perivascular spaces: analogy with Taylor’s swimming sheet. *J. Theor. Biol.* 523:110709
- Young BA, Adams J, Beary JM, Mardal KA, Schneider R, Kondrashova T. 2021. Variations in the cerebrospinal fluid dynamics of the American alligator (*Alligator mississippiensis*). *Fluids Barriers CNS* 18:11